Pekka Lehtinen

Projection microstereolithography equipment

School of Science

Thesis submitted for examination for the degree of Master of Science in Technology.

Espoo 12.2.2013

Thesis supervisor:

Prof. Matti Kaivola

Thesis advisor:

D.Sc. (Tech.) Jouni Partanen

Aalto University
School of Science

AALTO UNIVERSITY
SCHOOL OF SCIENCE

ABSTRACT OF THE
MASTER'S THESIS

Author: Pekka Lehtinen

Title: Projection microstereolithography equipment

Date: 12.2.2013 Language: English Number of pages:7+67

BIT Research Centre

Professorship: Engineering Physics Code: Tfy-125

Supervisor: Prof. Matti Kaivola

Advisor: D.Sc. (Tech.) Jouni Partanen

Stereolithography (SL) is one of the most successful additive manufacturing technologies. In SL a three-dimensional object is fabricated directly from a CAD model. The product is manufactured layer-by-layer by curing liquid resin. These layers, which are built on one another, form the product. In projection stereolithography (PSL) the laser light source and scanner system commonly used in SL, are replaced with a digital micromirror device (DMD) or a liquid crystal display (LCD). Thus, each layer is cured at once in one exposure according to the pattern on the DMD or LCD.

Projection microstereolithography (PμSL) operates on the same principle as PSL, but the fabrication resolution is significantly higher. In this study, a PμSL setup with a DMD chip is constructed and a computer code is written to control the entire manufacturing process.

Keywords: additive manufacturing, rapid prototyping, stereolithography, microstereolithography

AALTO-YLIOPISTO
PERUSTIETEIDEN KORKEAKOULU

DIPLOMITYÖN
TIIVISTELMÄ

Tekijä: Pekka Lehtinen

Työn nimi: Projektiomikrostereolitografialaitteisto

Päivämäärä: 12.2.2013 Kieli: Englanti Sivumäärä:7+67

BIT Tutkimuskeskus

Professuuri: Teknillinen fysiikka Koodi: Tfy-125

Valvoja: Prof. Matti Kaivola

Ohjaaja: TkT Jouni Partanen

Stereolitografia on menestyksekkäimpiä materiaalia lisääviä valmistusteknologioita. Stereolitografiassa kolmiulotteinen kappale tehdään suoraan CAD-mallista. Tuote valmistetaan kovettamalla nestemäistä resiiniä kerroksittain. Nämä päällekkäin kootut kerrokset muodostavat kappaleen. Projektiostereolitografiassa (PSL) laservalonlähde ja skanneri on korvattu DMD-sirulla (Digital Micromirror Device) tai nestekidenäytöllä (LCD), jolloin jokainen kerros kovettuu DMD:ssä tai LCD:ssä olevan kuvion mukaisesti kertavalotuksella.

Projektiomikrostereolitografia (PμSL) toimii samalla periaatteella kuin PSL, mutta kappale valmistetaan huomattavasti paremmalla tarkkuudella. Tässä työssä rakennetaan DMD:tä käyttävä PμSL-laitteisto ja kirjoitetaan tietokoneohjelma valmistusprosessin hallintaa varten.

Avainsanat: materiaalia lisäävä valmistus, pikavalmistus, stereolitografia, mikrostereolitografia

Preface

This Master's Thesis was done in the IDM (Integrated Design and Manufacturing) research group at the BIT Research Centre at Aalto University School of Science. I would like to thank BIT Research Centre for keeping me employed already for three years in a subject which greatly interests me. I am sure our cooperation will continue also in the future.

I would like to thank my supervisor Prof. Matti Kaivola for letting me use the Optics and Photonics Group's laboratory for my work and for providing academic insight. I also thank my advisor D.Sc. (Tech.) Jouni Partanen for introducing me to the world of additive manufacturing and stereolithography, as well as helping me throughout the microstereolithography project, constantly encouraging and supporting me. I would also like to acknowledge my colleague D.Sc. (Tech.) Harri Korhonen with whom I brainstormed during the construction processes of various stereolithography systems.

Finally, I thank my parents Anne and Tuomo, and my brother Juha for supporting me during my work and studies.

Otaniemi, February 12, 2013

Pekka Lehtinen

Contents

Abbreviations

2D	Two-dimensional
3D	Three-dimensional
μSL	Microstereolithography
AM	Additive manufacturing
CAD	Computer-aided design
CNC	Computer numerical control
CT	Computed tomography
DIY	Do it yourself
DLP	Digital light processing
DMD	Digital micromirror device
GUI	Graphical user interface
LCD	Liquid crystal display
MEMS	Micro electro-mechanical systems
MIP-SL	Mask-image-projection-based stereolithography
MIP-SLA	Mask-image-projection-based stereolithography apparatus
PDMS	Poly(dimethyl siloxane)
PI	Photoinitiator
PμSL	Projection microstereolithography
PμSLA	Projection microstereolithography apparatus
PSL	Projection stereolithography
RP	Rapid prototyping
RP&M	Rapid prototyping & manufacturing
SEM	Scanning electron microscope
SL	Stereolithography
SLA	Stereolithography apparatus
SLM	Spatial light modulator
SLS	Selective laser sintering
STL	Stereolithography CAD software file format created by 3D Systems
USB	Universal serial bus
VGA	Video graphics array

1 Introduction

Additive manufacturing (AM) is a manufacturing technology that is used to produce three-dimensional objects. The main principle of AM is that the structure is fabricated by adding material in layers. Usually this is done directly from a model that is created with a Computer-Aided Design (CAD) system. Thus, "3D printing" has become a common term for many AM processes, since essentially they "print" a 3D object according to the computer data.

There is a broad range of different additive manufacturing processes, which vary mainly in the material used. Materials range from plastics to metals and sand. For instance, plastics are used for stereolithography (SL) and metal powders for selective laser sintering (SLS). The material defines the layer creation method and the mechanical strength of the final product. AM processes also greatly vary in terms of accuracy and cost. Two-photon polymerization processes may reach resolution of sub-50 nm [1], while some inexpensive solutions stay in the mm range. The price of AM equipment often correlates with the fabrication accuracy and the material used. Inexpensive do-it-yourself (DIY) 3D printer kits may cost less than 1 000 €, while metal laser sintering devices may cost over 500 000 € [2]. [3]

Stereolithography (SL) is one of the most successful and oldest additive manufacturing technologies currently available. It was commercialized about 25 years ago. The main part of this technology involves curing or solidification of a liquid photosensitive polymer (also known as resin) with a light source. The curing reactions are initiated by laser light, which causes the small molecules in the resin to polymerize and crosslink. Thus, a solid layer is formed according to the scanned area of the laser. The finished structure consists of multiple cured layers that have been stacked upon each other. Between each layer one must apply a new fresh layer of liquid resin. This is usually done by moving the platform, upon which the structure is being built on, up and down. SL is known for high fabrication speed, part accuracy and surface finish. However, SL machines are expensive, due to the use of a laser and a scanner system, compared to various 3D printers [4].

By using a projection technique in SL, one may significantly reduce the equipment costs. The laser and scanner system are replaced by a dynamic mask generator, i.e., a liquid crystal display (LCD) or a digital micromirror device (DMD), and a lamp. The light emitted by the lamp is projected from the dynamic mask generator onto the resin. Thus, the resin will be selectively cured according to the pattern on the dynamic mask generator. An entire layer is manufactured at once, rather than vector by vector as in scanning SL. The projection stereolithography (PSL) technique lowers the machine cost and is more robust, since only one translation stage is required. [5]

Microstereolithography (μSL) is based on the same fabrication principle as SL,

but the fabrication resolution is better. The resolution is a few micrometers both in the lateral and vertical direction. Originally μSL was developed to produce high precision 3D MEMS (micro electro-mechanical systems) [6, 7]. However, μSL can be used to produce useful components for microfluidic, microrobotic and biomedical applications. For instance, artificial blood vessels could be made by combining 3D printing technology and two-photon polymerization [8], which may also be possible using high performance μSL equipment. Projection μSL (PμSL) equipment can be constructed similarly to a PSL system to reduce the equipment cost and increase the fabrication speed.

The goal of this study is to construct a projection microstereolithography system that is capable of producing structures with a few micrometers accuracy and write a computer program to control the entire process. Basically, the PμSL equipment consist of a video projector, various optical components, resin vat, a linear translation stage with a platform and a computer. Before the manufacturing can begin, some preparations must be done. First, the CAD model is sliced into horizontal cross-section images. These black and white images will be projected one by one onto the resin. The computer program will handle the changing of images as well as sending movement commands to the stepper motor that moves the platform upon which the part is built. It is important that the image projection and platform movement are synchronized to avoid part manufacturing failures. Before the actual manufacturing process, the computer program should accept several input parameters, such as layer thickness, motor movement speed, exposure time and image projection size. These parameters make the equipment versatile and suitable for a wide range of different tasks.

To achieve a uniform exposure some adjustments must be made to the images. By applying an intensity corrected grayscaled background image to all the sliced images, one can correct for spatial inhomogeneities in the output of the light source. Uniform exposure is important to acquire precise control of the curing process.

For reaching micrometer resolution, the lateral dimension of each projected pixel should be in the μm range. The properties of the resin must also be taken in account, since the vertical resolution is highly dependent on them. The equipment constructed in this study are based on a bottom-up approach, where the cured layer is formed between the bottom of the resin vat and the platform. Thus, the bottom of the resin vat should be non-sticky so that the cured resin layer does not get attached to it. The setup is constructed using commercially available and self-made components aiming at a minimum of cost, which would ease the spreading of PμSL technology to other research groups in the future.

2 Additive Manufacturing

A variety of industries use the term Rapid Prototyping (RP) to describe a process for rapidly creating a part or system representation before commercialization or final release. As the term RP implies, the idea is to create something quickly and the output usually is a prototype or basis model from which further models and eventually the final product will be derived. Commonly, in a product development context the term RP is used to describe technologies that create physical prototypes directly from digital data. [4]

As the RP technologies have evolved, the users of RP have realized that the term is inappropriate, since it does not accurately describe the more recent applications of the technology. RP machines have experienced major improvements in output quality and today they may produce real products instead of only prototypes. The basic principle of these technologies, which is part fabrication in an additive manner, is also overlooked by the term RP. Nonetheless, RP is still commonly used. [4]

The basic principle of additive manufacturing (AM) technology is that the part is fabricated directly from a model by adding material in layers. The model is usually created using a three-dimensional Computer-Aided Design (3D CAD) system. Each layer added upon the previous one is a thin cross-section of the part derived from the CAD data. The thickness of the layers determines how closely the resulting part corresponds to the original data. The thinner the layers are, the more layers must be fabricated, which may increase the manufacturing time, but the result will be of higher quality. All commercialized AM machines use a layer-based approach, but they differ in the materials that can be used, the layer creation method and the bonding of layers to each other. These differences will determine the material and mechanical properties along with accuracy of the final product, as well as the part manufacturing speed, the size of the AM machine, the requirement of post processing and the overall cost of the machine and process. [3, 4]

With the help of AM technology, a 3D object can be copied with ease. A three-dimensional digital model of the object can be created using a 3D scanner or by taking several photographs from different angles and combining them into a model. This model can then be fabricated using AM techniques. The complexity of the scanned object does not produce any additional costs or limitations.

There is a set of sequenced tasks that the user has to go through when an AM machine is involved in the product development process. However, in some AM solutions the task sequence is simplified to such an extent that the operator only has a few options to choose from and the part is manufactured with minimal effort. These machines are user friendly, but also limit the manufacturing choices regarding materials or variables to experiment with. The difficulty to operate increases as the machine becomes more versatile, but an experienced operator may put the large

variety of parameters to good use. Regardless of the AM machine, the process can be divided into eight key steps as done by Gibson *et al.* [4]:

1. Conceptualization and CAD
2. Conversion to STL (triangular representation of the CAD model)
3. Transfer and manipulation of the STL file to the AM machine
4. Machine setup
5. Build
6. Part removal and cleanup
7. Post-processing of the part
8. Application

Depending on the equipment or the perspective of the user, there may be more steps or substeps, but these eight steps are fairly general. [4]

Initially, AM was mostly used for creating visualization models for products while they were developed. 3D physical models can be much more helpful than drawings in understanding the design of the object and the intent of the designer. The case where two twin sisters, joined at the head, serves as an example. They were separated the 24th of July 2001, and for that a 3D model (an STL file) was created for RP by taking several CT scans from various directions. A model of the intersection of the two skulls was fabricated, which helped the surgeons to plan the surgery and how they would reroute the vital blood vessels. Thanks to the planning, the operation took only 22 h to complete, while similar procedures may take even 97 h. [4, 9]

The geometric description can be conveyed from a CAD to the AM process in various formats. However, the STL (STereoLithography) has become the most used file format in AM techniques. The STL file was originally conceived by 3D Systems Co. and it opened the door for RP&M (Rapid Prototyping & Manufacturing) market by allowing CAD data to be used in SL systems. The file consists of an unordered list of triangular facets that represent the outside skin of a part (see Fig. 7.14(a) for an example). The triangular facets are described by a unit normal vector and a set of X, Y, Z coordinates for each of the three vertices. The unit vectors indicate the outside of the part. Since the STL model consists of triangular facets, it is an approximate model of the accurate CAD data. Regardless of being an imprecise model, STL has become the standard used by most CAD and RP systems. STL is a simple solution for representing 3D CAD data and it provides small and accurate

files for data transfer for specific shapes. [9, 10]

However, in some cases the STL file may be many times larger than the original CAD file for a certain accuracy parameter, since the STL file may carry unnecessary redundancy such as duplicate edges and vertices. Geometry flaws may exist in the STL file, which gives rise to a demand of "repair software", which again slows down the production cycle. The slicing of large STL files can take many hours, but in some RP processes the slicing can occur while the previous layer is still being built. [9]

The printing software should be able to control both the movement of the translation stage and the image exposing process. No image should be exposed when the motor is moving, and the exposure time should be adjustable. The CAD model contains all the data required by the computer to produce an exact 3D replica.

The 3D printer software starts by examining the CAD model and calculating the best method of printing it with using the least amount of time and material. For instance, hollow structures may require an inner structure to be rigid. The software will design the interior structure that resembles a honeycomb. This will minimize the material use without neglecting the mechanical strength of the structure. Once the printing method has been chosen the software slices the model into horizontal layers as thin as the printer can handle. Each of these slices will then be used to control the printing process. After one layer has been printed the software commands the z-motor to move and the printing of the next layer may be initiated. [11]

AM technology has evolved from the days when it was only useful for model making. The technology developed as materials, accuracy and quality of the output improved. AM can be used in conjunction with other technologies to significantly shorten product development times and costs. In some cases, the output is directly suitable for end use.

AM technologies can be used in a large variety of fields. For instance, AM technology has been successfully utilized in the medical field by Dr. Stephen Rouse who runs the Walter Reed Army Medical Center's 3D Medical Applications Center. He is a pioneer at repairing severe skull injuries through individualized and additive manufactured implants. Another example is a process entitled Contour Crafting, automatized construction of buildings. This AM process is developed by Prof. Behrokh Khoshnevis from the University of Southern California, USA. The basic idea of Contour Crafting is that a house can be made additively using concrete. With this method it may be possible to build a house in one day or a whole block of houses rapidly and cost efficiently. Or you might even print your food using a 3D printer, which may be called a "food printer". For instance, researchers at the University of Exeter have developed a 3D printer that uses chocolate instead of ink or plastic. [12, 13, 14]

AM technologies are becoming more and more common in everyone's daily life. The cost efficiency is unmatched in many fields since AM is material efficient and no transportation is needed if the users can print the part they need at home or in some nearby 3D print shop. Some even speak of a possible revolution in the field of product development and manufacturing. Some claim that manufacturing as we know it today might not exist if we follow AM to its ultimate conclusion. There are plenty of factors that could make a revolution possible. [4, 11, 15]

First, the manufacturing speed does not only reduce the manufacturing time of a product, but also the entire product development process. The transfer from a 3D CAD file to AM is relatively seamless, which significantly reduces concern over data conversion or interpretation of the design intent. Due to the seamlessness there are only a few process steps in the manufacturing process. The complexity of the product does not impose any time consuming procedures. Other manufacturing processes may require multiple and iterative stages before the object can be manufactured as intended. The number of these stages usually increases dramatically as more features are added to the design. However, in AM the time required to fabricate the model can be effectively predicted, regardless of the complexity of the object and the added changes during the formative stage of product development. Comparing AM with a common crafting process, the advantages of AM become evident. [4]

Manufacturing a prototype from a CAD drawing by a skilled craftsman may require a number of steps, since the craftsman must employ a variety of construction methods ranging from CNC (Computer Numerical Control) machining, through molding and forming, to precise hand carving. CNC machining requires a sequential approach and detailed planning, which may demand construction of fixtures to ease the manufacturing process. CNC reminds of AM, since the part is manufactured based on a computer model. However, CNC is a subtractive technique, while AM is an additive process. Thus, CNC requires a block of material, which is larger or the same size as the manufactured part. AM, on the other hand, can build the part with less or equal amount of material than the volume of the part since the interior structure does not have to be solid. Molding processes require the building of one or more molds and can be messy. Hand carving is tiresome, laborious and prone to error. All these techniques should be within the repertoire of the craftsman, for part manufacturing. AM can simplify many of these mentioned stages or remove them completely. [4]

The maker movement is becoming stronger, since objects can be made by individuals themselves instead of buying already made products that lack uniqueness and personality. The product has always greater value for the user if it is self-made or some contribution has been done in the manufacturing process. This is one of the major advantages of AM, as you can manufacture a product just like you want with only your imagination as the limit. [11]

3 Light induced reactions in polymers

3.1 Photopolymerization

Polymerization refers to the process in which molecules of small molar mass and short chain length (monomer) form a polymer structure with longer chains and greater molar mass. Polymerization of a vinyl-type monomer is presented in Fig. 3.1. The carbon-carbon double bond is a functional unit. Each carbon atom in the double bond may form a new bond with another, usually carbon atom of a different monomer molecule. As the weak van der Waals interactions of neighboring molecules change to a network of covalent bonds, the bulk properties change. The shear strength increases as new bonds form and the system changes from liquid to solid. Besides single bonding, multifunctional monomers may form crosslinks in the polymerization process. The monomer is called multifunctional if the molecular structure (depicted as R) contains multiple vinyl groups. [10, 16]

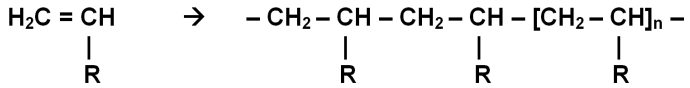

Figure 3.1: Polymerization of a vinyl-type monomer through double-bond opening. [10]

A photochemical event initiates the chain reaction in light-induced polymerization. Photoinitiators absorb light of a specific wavelength and initiate the photopolymerization of the photosensitive material. [16]

The photopolymerization reaction may be described with four steps: initiation, association, propagation and termination. Photopolymerization reaction mechanisms are presented in Eqs. (1)-(6). The energy of the absorbed photon is denoted as $h\nu$. Reaction rates are presented with k and the subscripts designate different processes (e.g. in k_{tr} the subscript stands for termination by recombination). [10, 16]

$$PI \xrightarrow{h\nu} PI^* \rightarrow R^* \tag{1}$$

$$R^* + M \xrightarrow{k_1} P^* \tag{2}$$

$$P^* + M \xrightarrow{k_p} P^*_{n+1} \tag{3}$$

$$P^*_n + P^*_m \xrightarrow{k_{tr}} P_{n+m} \tag{4}$$

$$P^*_n + P^*_m \xrightarrow{k_{td}} P_n + P_m \tag{5}$$

$$P_n^* + P_m^* \xrightarrow{k_{to}} P_n^* + P_m^* \tag{6}$$

In the initiation step (Eq. (1)), the photoinitiator (PI) is excited by absorption of a photon of appropriate frequency and produces radicals (in the case of radical polymerization). In the association step (Eq. (2)), the monomer species transform into a growing polymer. The conversion is induced by an active radical. In the propagation step (Eq. (3)), the polymer lengthens by continuous addition of monomers until termination occurs. The termination may happen in three different ways (Eqs. (4, 5, 6)). In recombination (Eq. (4)), two radicals join to form a nonreactive molecule. In disproportionation (Eq. (5)), one radical transfers a β-hydrogen to another and thus two polymer molecules are formed. It is also possible that even long after the radiation some unreacted radicals are present. This "frozen mobility" or occlusion (Eq. (6)) is a major termination pathway for SL resins. [10, 16]

In addition to radical photopolymerization, as described above, there are two other classes of photoinitiation: hydrogen abstraction and cationic polymerization. The basic polymerization mechanism (Eq. (1)) holds also for cationic polymerization. However, a carbocation (a positively-charged carbon atom) will be formed in the initiation process, as opposed to radical-induced polymerization. Acidic species are produced when the cationic photoinitiator is affected by light. The polymerization process is initiated by the reactions between the acidic species and monomers. Due to the protonic acids, cationic photoinitiators may not be used in, e.g., tissue engineering applications. In hydrogen abstraction, the photoinitiator abstracts a hydrogen molecule from an H-donor and generates a ketyl radical and a donor radical. The H-donor radical often initiates the photopolymerization, while the ketyl radical couples with the growing macromolecular chains. [16, 17]

3.2 Photocrosslinking

It is possible for a crosslinked polymer network to form if the monomer contains more than one reactive functional unit, i.e., the monomer is multifunctional. Photocrosslinking differs from photopolymerization, since photocrosslinking concerns the formation of covalent bonds between oligomers (already polymerized molecule chains) often through a double-bond opening, which is presented in Fig. 3.2. In this process, the viscosity of the material increases dramatically and it becomes solid. In photocrosslinking every chain progression step requires the absorption of a photon, unlike in photopolymerization. [16, 18]

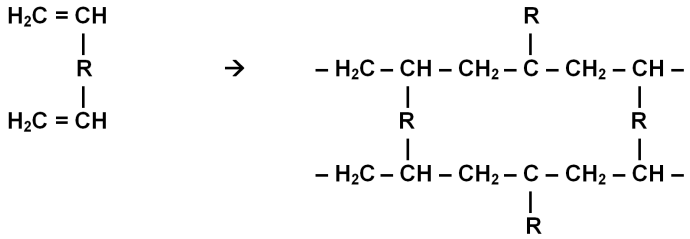

Figure 3.2: Crosslinking [10]

3.3 Photopolymers and stereolithography

Photopolymers were developed in the late 1960s and shortly thereafter they became widely applied in various commercial areas such as the coating and printing industry. For instance, glossy coatings on paper can be achieved with photopolymers and in dentistry photocurable resins are used for filling deep grooves and preventing cavities. In these cases the curing process is done without patterning, since it is not required. When patterning was applied to the curing process, it led to the introduction of stereolithography. [4]

Charles (Chuck) Hull experimented with UV-curable materials in the mid-1980s. He exposed the materials to a scanning laser, which operates in the same manner as the ones found in laser printers. He realized that it was possible to produce solid polymer patterns. He could also fabricate a solid 3D structure by curing one layer over a previous one. This was the starting point of SL technology. Soon after the discovery, 3D Systems was created to market SL machines as RP machines for the product development industry. Since the late 1980s an abundance of SL-related processes and technologies have been developed. [4]

3.4 Photocuring

The word curing refers to solidification of a polymeric solution. RadTech North America defines radiation curing in the following manner: "radiation as an energy source to induce the rapid conversion of specially formulated 100 % reactive liquids to solids". Curing is achieved in most cases with UV or visible light, but in some occasions it is possible to utilize electron beams, x-rays, γ-rays, plasmas and microwaves for it. [18]

A photocurable resin consists of a photoinitiator, monomers, oligomers and additives. Once affected by light the photoinitiator generates radicals that react with the neighboring monomers. This process is radical-induced polymerization, as in the case where acrylate resin polymerizes. In cationic polymerization, on the other hand, an epoxy resin is polymerized by cationic ions. These processes differ in the

photoinitiation reaction as previously explained. [19]

The first photocuring units were introduced in the early 1970s. They were designed to operate with ultraviolet light. The units were very successfully (speed, easiness) applied for curing dental restoratives. Visible light came along to the photocuring processes a few years later (1976). It must be taken into account that the change of wavelength demands for different photoinitiators and other changes may be necessary for the curing to be efficient. [20]

The curing process initiates when the emitted photons react with the photoinitiators in the resin, but the exposure must be sufficient. Exposure is defined as radiant energy per unit area (usually $\mathrm{mJ/cm^2}$). Photopolymerization will not proceed beyond a certain depth if the light exposure is below a threshold value. The exposure requirement for gel (not fully solid, but not liquid) formation is known as critical exposure (E_c). [10]

The liquid resin is usually held in a container when radiation is applied. If the exposure is high enough, the resin will be cured thoroughly from the surface to the bottom at the exposure spot. Thus, by altering the distance between the resin surface and a movable platform, one can control the thickness of the cured layer. Depending on the setup this can be done in different ways as will be discussed in Sec. 4.2. The curing rate decreases as the concentration of unreacted monomers decreases and the viscosity of the gel increases. As a result, the curing depth decreases exponentially. Light absorption of the resin can be described by the Beer-Lambert law,

$$\mathrm{E}(z) = \mathrm{E}_0 e^{-\frac{z}{\mathrm{D}_p}}, \tag{7}$$

where E is the exposure, z is depth (z=0 on surface), E_0 is the exposure on the surface and D_p is the light penetration depth of the resin. [10]

The composition of the resin and especially the photoinitiator used may cause deviation from the exponential law. For instance, photobleaching causes the curing depth to be greater than expected. Inhomogeneousity (optically) may induce scattering and therefore the penetration depth will decrease, but the lateral curing area may increase. [10]

In stereolithography the object is manufactured layer-by-layer. The layer thickness may be adjusted by mechanical means, i.e., by moving the platform, upon which the structure is being built on, up or down. However, the curing depth is difficult to alter if the object has overhanging parts (i.e. bridge-like structures, where the new layer is larger than the previous layer). To stop the curing process at a desired depth, one may have to utilize neutral absorbers.

3.5 Utilization of neutral absorbers

Besides photoinitiator molecules, it is possible to add neutral absorbers into the resin to absorb photons. The term "neutral absorber" is used, since the absorber absorbs light and dissipates the captured energy without interfering with the polymerization process itself. Neutral absorbers are especially efficient in reducing the polymerized thickness of the resin. The neutral absorber can be a coloring dye, which absorbs photons of a small range of frequencies. To minimize the absorber concentration, the absorber should be chosen so that the peak absorption is near the operation wavelength of the system. The downside of neutral absorbers is that they reduce the reactivity of the resin. [21]

Along with neutral absorbers, one may adjust the curing depth by controlling the exposure time, due to the exponential decay. Reducing the exposure time is not always sufficient for achieving low curing depth, since the light may penetrate far into the resin even in a short amount of time. Thus, it is essential to alter the properties of the resin to reduce the penetration depth. Adding a neutral absorber into the resin reduces the polymerized thickness of the resin, but the required energy to initiate the curing process is increased. This is troublesome, if the initiation threshold of polymerization becomes too high for the used light source. Thus, polymerization may not occur at all. Increasing the exposure time may solve the situation, but long exposure times lead to low fabrication speed. [21]

The mechanical strength of the final product does not alter significantly by the addition of an absorber, since even a concentration of few per mil of absorbing molecules is enough to reach remarkable changes in the penetration depth. However, if the absorption peak of the neutral absorbers is not matched with the light source, a high concentration of neutral absorber is required to reduce the curing depth significantly. High concentrations of material not taking part in the polymerization may affect the mechanical strength.

4 Photopolymer-based additive manufacturing techniques

The main configurations that have been developed for photopolymerization processes can be categorized in the following manner (as done by Gibson *et al.* [4]):

- *Vector scan*, or *point-wise scan*, which is a typical approach in commercial SL machines
- *Mask projection*, or *layer-wise irradiation*, where an entire layer is irradiated at once
- *Two-photon irradiation*, which is used in high resolution point-by-point approaches

These configurations will be looked into via some example approaches in the following sections.

4.1 Stereolithography

Stereolithography (SL) is an Additive Manufacturing (AM) technology, which was commercialized in 1987. Stereolithography was a pioneering method in RP&M technology and it was commercialized by 3D Systems Inc. The advantages of stereolithography are its versatility in manufacturing parts with different geometries and dimensions, its quickness and its accuracy. [22]

Laser scanning is used in stereolithography to manufacture three-dimensional objects. The laser scans the surface of a liquid resin and the resin gets cured according to the scanned pattern. These successively cured resin layers form the part. This type of stereolithography can be categorized as scanning stereolithography, since the parts are constructed in point-by-point and line-by-line fashion. An illustration of a stereolithography apparatus (SLA) is shown in Fig. 4.1. [22, 23, 24]

As in all radiation and layer-based AM processes, several phenomena are common to SL. The part consists of layers of finite size, which causes slanted or curved surfaces to have "stair steps". Afterwards the part can be finished by removing material that is outside of the desired geometry. Individual pixels and laser scans are rarely visible on the part surface. [4]

Illuminating a layer will cure the irradiated areas and the liquid resin becomes solid, which results in shrinkage. Individual monomers occupy a larger volume than polymers. This is common also in SLS where the volume of melted sand or metal

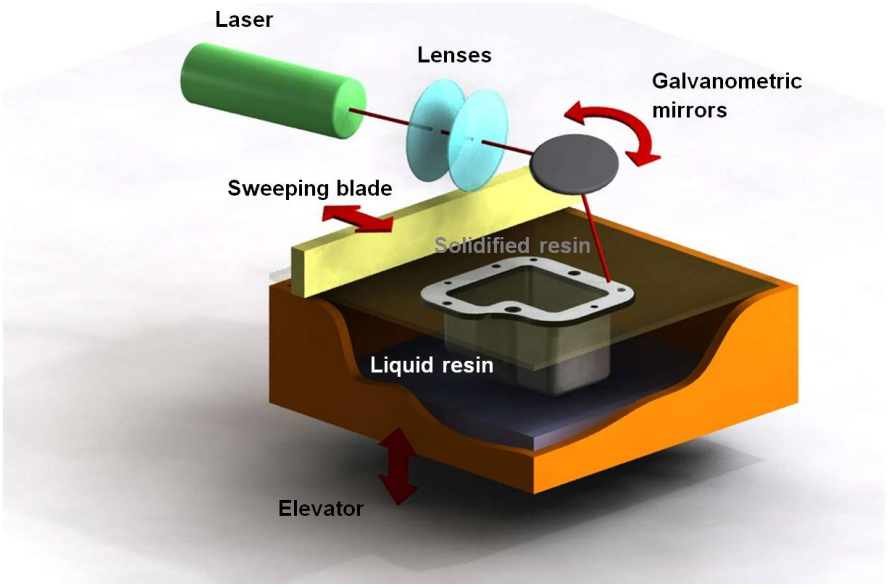

Figure 4.1: An illustration of a stereolithography apparatus by Roy Björkstrand, BIT Research Centre.

reduces as the material freezes. The shrinkage of one layer causes stress to layers next to it. This stress can build up as more layers are fabricated. The stress may not affect the appearance, but it can also cause cracks in the part or the part edges may curl upwards. [4]

Curing a new layer may affect the previous layers, since the extra energy that extends below the current layer causes undesired extra layer thickness. This phenomenon is called print-through error in SL or "bonus Z" in laser sintering. [4]

4.2 Projection stereolithography

The laser of a SLA can be replaced with a projection-based light source. A digital micromirror device (DMD) or a liquid crystal display (LCD) can be used as a dynamic mask to achieve an integral curing approach to the layer creation process. The reflected light from the DMD is shaped according to the defined mask pattern. The modulated light is then focused onto the resin using optical components. This projection method in SL may be referred to as mask-image-projection-based stereolithography process (MIP-SL) or as projection stereolithography (PSL). [25, 26, 27]

A DMD consists of hundreds of thousands of small mirrors. Each mirror corresponds to a pixel that can be independently turned on or off. Therefore, it is possible to use a light projection device to project a dynamically defined mask image onto a resin surface and selectively cure the layer according to the projected image. The

main advantages of DMD over LCD are smaller pixel size and narrow gaps between pixels. DMD also has higher switching speed than LCD, which is important in grayscale intensity modulation at pixel level. DMD is also UV compatible whereas LCD is not. [25, 26]

In a top-down projection approach, which often is the same as a free surface technique, such as in Fig. 4.1, the resin is cured at the resin surface by light coming from above. Thus, the layer thickness is determined by gravity, viscosity and surface tension, i.e., the amount of fresh resin deposited on the surface of the structure. The thickness of the resin layer on the structure may also vary when the number of cured layers increases if the shape of the top part of the cured object near the surface is different. Therefore, it is necessary to use a sweeping blade to smoothen the resin surface unless the resin has a very low viscosity. Using a sweeping blade to smoothen the surface is time consuming and prevents fast building speeds. Oxygen inhibition is an issue if the surface of the resin is in contact with air [10]. The outermost layer of the cured object will not be completely cured due to oxygen. The problem with spreading fresh resin and oxygenation can be overcome by adding a glass window onto the resin surface. Thus, curing occurs through the transparent window, but a major drawback is that the cured layer may stick to the glass. [21]

Besides the top-down projection approach, another viable approach is the bottom-up projection approach, which is shown in Fig. 4.2 for a PSL process. In this approach the bottom of the tank must be transparent, since the mask image is projected from below. The layer thickness can be accurately determined by the gap between the platform and the bottom surface of the tank. The layer thinness is only limited by the movement accuracy of the motorized translation stage. The bottom-up-based system has multiple advantages over the top-down-based approach with a free surface. Firstly, as mentioned above, recoating is achieved by constraining the fresh resin layer between the previous layer and the bottom surface of the tank. Thus, no sweeping is required and the layer thickness is determined with high accuracy regardless of the resin viscosity. Secondly, the part height is independent of the container depth. Thirdly, oxygen inhibition is eliminated. [26]

The major downside of a bottom-up projection system is that the cured layer may stick to the resin vat, which will prevent object manufacturing. The same problem is present in the top-down approach when the light cures the resin through a glass window. Thus, one must find ways to reduce the attachment to the vat, which can be done by coating the vat with a suitable non-sticky material or by detaching the cured layer by slightly tilting the resin vat to reduce the pull up force.

The use of a projector as the light source offers the user the option to choose the wavelength from a wide spectrum. A narrow band-pass filter can be used to select a specific wavelength to match the currents needs, for instance, the absorption peak of the photoinitiator.

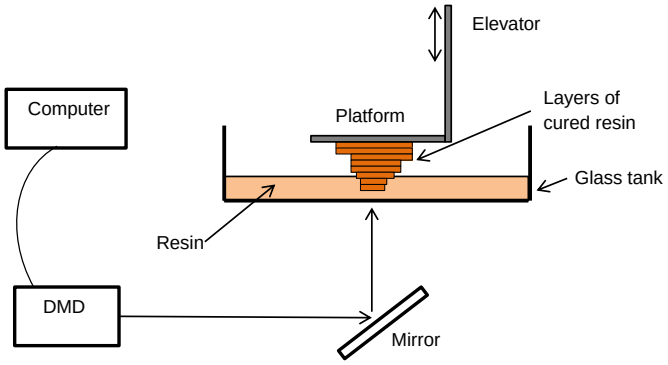

Figure 4.2: An illustration of a bottom-up-based projection stereolithography apparatus.

4.3 Microstereolithography

The manufacturing principle is the same in microstereolithography (μSL) as in stereolithography. However, the resolution of microstereolithography is far better than in most other rapid prototyping techniques. Stereolithography has a typical resolution of 150 μm in the three directions of space, while in μSL it is around a few micrometers. High resolution and rapid manufacturing are the main advantages of μSL, which make it appealing for both rapid prototyping and microengineering. [21]

Research teams who published the first scientific reports on μSL used many different designations (IH process, spatial forming, 3D optical modeling, microphotoforming, microstereophotolithography, etc.) due to a possible variation in the design in the apparatuses built. Nowadays, the name "microstereolithography" is accepted by almost all users and developers, as it connects the manufacturing process both to the stereolithography and microfabrication fields. [21]

The first μSL system was developed by Ikuta *et al.* in 1992. It was named IH process (Integrated Harden Polymer Stereolithography). It was used successfully to fabricate bending pipes, micro coil springs, artificial venous valves and other real micro structures made of polymer. [28]

There is an increasing need for small size prototype parts of high resolution as the market for miniaturized products broadens. Microstereolithography can produce useful components for the microfluidic, microrobotic, microsystems and biomedical fields. The components produced by μSL are also used in combination with components made by other methods to achieve a special function to the assembly in a microsystems device. [21]

Microstereolithography is not yet commercially available even though a few ser-

vice bureaus are using it to manufacture small high-detailed objects that cannot be produced by other rapid prototyping technologies. Fabricating MEMS devices is one of the promising applications of μSL. [21]

Microstereolithography and SL are not limited to using only polymers. In the field of SL, ceramic particles have been embedded in a photopolymerizable polymer matrix to create large-sized prototype parts in composite materials and to fabricate ceramic parts that can be used as functional components or as molds for investment casting. Ceramic microfabrication by μSL was successfully demonstrated by Zhang *et al.* in 1998 [6]. Microceramic structures are keys to high temperature and corrosion resistant MEMS devices. [6, 21]

Bertsch *et al.* developed a μSL machine that could utilize a photopolymerizable medium containing a high load (up to 80 wt%) of alumina nanoparticles. The manufactured composite objects can undergo a debinding and sintering process to be transformed into pure ceramic microcomponents. During the transformation the shape of the objects does not alter, but shrinkage is an issue. However, if the load of the filler material is high enough in the resin, no cracks or deformations can be seen in the final ceramic products. [21, 29]

Recent improvements of the μSL process are related to development of new usable materials. Biocompatible or biodegradable polymer-based resins as well as composite, ceramic and metal materials contribute to the further evolution of nano and microsystems towards biomedical applications. [21]

4.4 Two-photon polymerization

Two-photon polymerization method differs from vector scan and projection techniques, since the part is manufactured directly inside the reactive medium. Thus, no moving platform is needed for the cured layers to be attached to. No support parts are required and there is no need for spreading liquid on the manufactured parts. Due to these properties it is not necessary to manufacture the part by piling up two-dimensional layers. [21, 30]

Three-dimensional microfabrication with two-photon polymerization was proposed by Maruo *et al.* in 1996. The technology is often referred to as two-photon microstereolithography. [21, 30]

Two-photon absorption is a nonlinear phenomenon which occurs in any material if the irradiance is adequately high and the transition energy between the ground state and an excited state are matched by the combined energy of the two photons. The two-photon absorption rate is proportional to the square of the incident light intensity. This quadratic dependence confines the phenomenon to occur at the

focal point, which in turn confines the photopolymerization process into submicron volumes. [21, 30]

With two-photon photopolymerization it is possible to manufacture structures with feature sizes beyond the diffraction limit. While using a titanium sapphire laser operating at 780 nm, the diffraction limit can be exceeded by nonlinear effects to achieve a sub-diffraction limit spatial resolution of 120 nm. A "micro-bull" sculpture is presented in Fig. 4.3. The bull is 10 µm long and 7 µm high. Same-sized micro-machines could be transported through even the smallest blood vessels inside the human body. For instance, this would be useful for delivering clinical treatments. [31]

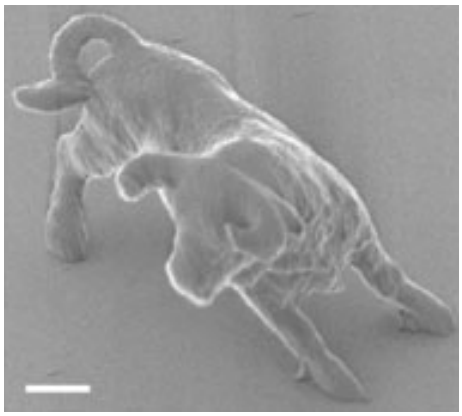

Figure 4.3: A micro-bull sculpture manufactured using two-photon absorption. The scale bar corresponds to 2 µm. Adapted from [31].

5 Resolution in projection stereolithography

5.1 Lateral resolution

Lateral resolution in projection stereolithography is primarily defined by the used optics. Decreasing the spot size of the focused light beam at the working platform leads to higher resolution. The focusing can be done by using a microscope objective, which can produce 1 µm sized details. The sizes of the mirrors in the DMD also affect the resolution. Once the setup has been built, one can enhance the lateral resolution by making sure that the exact focus is on the working platform. Increasing the numerical aperture will lead to a higher resolution, but the depth of the focus will simultaneously decrease. A short depth of focus causes irregularities in the vertical direction. Instead of a constant lateral exposure the cured layer would be hourglass-shaped if the depth of the focus is shorter than the layer thickness. Therefore, the depth of the focus should be larger than the layer thickness.

It is also crucial to use the right exposure time, since over-curing will blur all the details. The properties of the used resin may also affect the resolution if chain reactions in the resin are powerful. The polymer may get cured even outside the lit area due to chain reactions and light scattering, which may be referred to as the cross-talk effect [25]. Light affecting the resin will always get slightly scattered and diffracted. The lateral resolution decreases with over-curing, since even the scattered light, which does not usually play a significant role, will lead to curing. Thus, the cured shape will get larger than intended and the smallest details will be blurred. The reduction in resolution, due to these phenomena, is not very strong when only a few layers are cured, but manufacturing multiple layers causes the blurring to become more severe. The problem arises especially if the uncured resin, which remains near cured structures, does not get replaced with completely fresh resin. This happens easily when the resin is viscose. Resins of low viscosity are able to flow into smaller structures and holes, which makes them appropriate for microstereolithography.

5.2 Vertical resolution

Once light interacts with the resin, the curing process initiates. The minimal thickness of the cured resin is often greater than the cured dimension in the lateral direction, because the vertical resolution depends primarily on the properties of the resin, which are hard to control compared to the lateral curing. Reducing the layer thickness by adding a thinner layer of resin on the structure being built does not enhance the vertical resolution. Controlling the layer thickness enables the structure to have smooth edges, but the vertical resolution is determined by the overhanging

parts. Finding ways to control the penetration of light is crucial for enhancing the vertical resolution.

The wavelength of light is an important factor affecting the resolution. The wavelength determines the resolution limit, which is theoretically achievable. Short wavelengths get absorbed in a thinner layer than long wavelengths. UV light is, therefore, often used in stereolithography applications. In a projector-based setup the shortest wavelength that has been used is at around 420 nm, which is sufficient for reaching 1 µm resolution in practice. The broad spectrum of a projector lamp allows one to change the operation wavelength easily with narrow bandpass filters. Variation of the wavelength provides a tool for controlling the curing depth.

Having a resolution goal of 1 µm in the vertical direction usually requires altering the properties of the resin. Neither free surface nor constrained surface approaches affect the resolution of overhanging parts. In Fig. 5.1 is presented the problem of long penetration depth. The penetration depth may be reduced by, e.g., adding neutral absorber into the resin. The resolution of overhanging parts is determined by how sensitive the resin is to light, the exposure time and the used optics. The exposure time may be controlled with high accuracy using a computer. It is also possible to change the power of the light, but in a projector-based system changing the exposure time is more convenient. In a laser-based setup changing the power is a more commonly used method. Adjusting the light sensitivity to control the polymerization is a chemical process, which can be done by adding light absorbing additives.

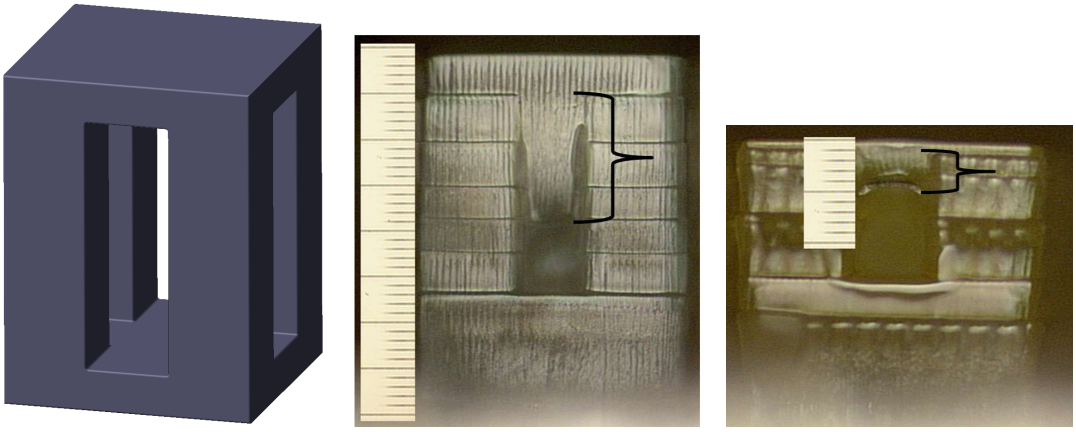

Figure 5.1: A designed object with an overhanging roof and two manufactured replicas. The print-through error is significant in the first manufactured structure. Adding neutral absorber has reduced the print-through error from 150 µm to around 40 µm in the second structure.

By manufacturing multiple structures containing overhanging parts using different exposures, it is possible to achieve experimental "working curves" for the curing

process. The curing depth depends on the properties of the resin and the exposure energy. From the Beer-Lambert law (Eq. (7)) it is possible to derive the working curve equation,

$$\mathrm{C}_d = \mathrm{D}_p \ln \frac{\mathrm{E}_{max}}{\mathrm{E}_c}, \tag{8}$$

where C_d is curing depth, D_p penetration depth, E_{max} maximum exposure and E_c critical exposure. The parameters D_p and E_c are constants of the resin. Plotting C_d versus $\ln(\mathrm{E}_{max})$ should yield a straight line with a slope of D_p and an exposure intercept of E_c. The parameter D_p describes the minimum achievable curing depth. By adjusting the resin properties and by optimizing the exposure time one may reach 1 µm in the curing depth. [10]

Finding the right composition for the resin requires multiple experiments with different resin properties. Determining the penetration depth with the working curve equation is quite laborious, since it demands multiple curing experiments with different exposure times and accurate thickness measurements. It may be more reasonable to test each resin with a few simple experiments. The lowest curing depth can be found quite quickly by manufacturing structures with overhanging parts. The top layer (overhanging part) is manufactured with the smallest possible exposure time. After a few trials one should have found the shortest exposure time which produces a completely cured layer. By analyzing this layer thickness one may determine the lowest curing depth.

6 Existing projection microstereolithography systems

Research in the field of PμSL is mostly experimental in nature, since PμSL is a relatively new technology and there is a large variety of approaching methods. This chapter will look into three different PμSL systems that vary among other things in the choice of the light source. However, the main difference between these approaches is in the dynamic mask.

6.1 LCD as a dynamic mask

The idea of using PμSL with an LCD mask was first demonstrated by Bertsch *et al.* in 1996 (published 1997 in Journal of Photochemistry and Photobiology A: Chemistry). They used a laser beam which was expanded with a beam expander to illuminate the largest possible surface of the LCD. The pixels in the LCD that are in their opaque state stop light while rest of the pixels remain transparent. Thus, as the light passes through the LCD it will contain the pattern of the layer. After the LCD the beam passes through a beam reducer and is focused onto the surface of the resin. The system operated in the visible light range, and used the top-down approach. The z-motor was the only mobile element in the setup. [32]

The downsides of this approach are low resolution and contrast of the LCD. Only a circle containing a small number of pixels on the LCD are usable, which prevents very high precision manufacturing of parts. The pixels in their opaque state let about 20 % of the light pass, which demands use of a chemical medium with a polymerization threshold. Thus, organic dye was added to the resin. However, the dye was affected by photobleaching, which means that polymer formation propagates deeper and deeper in the resin as the dye is bleached. Thus, controlling the polymer formation in the vertical direction became more challenging. Due to the delicate nature of the micro objects, no scraper could be used to add a new layer of reactive medium. Thus, it was necessary to use low viscosity resins. In spite of the limitation of the LCD and the use of a chemical medium with a polymerization threshold, a resolution better than 5 μm in the three space directions was achieved. [32]

6.2 SLM as a dynamic mask

Instead of using an LCD as mask, Farsari *et al.* used a spatial light modulator (SLM). Each slice of the 3D model was converted into a bitmap and loaded onto the SLM, which acted as a dynamic lithographic mask. The SLM was a special LCD component, which was not damaged by wavelengths longer than 350 nm. The mask was illuminated using a UV laser light source operating at 351.1 nm. The SLM had

a resolution of 800×600 with a pixel size of 26 µm × 24 µm. The pixel fill factor was 50 % and the contrast ratio was 200:1 with a grayscale modulation of at least four levels. Before the SLM, the nominally Gaussian irradiance distribution of the laser beam was reshaped to a rectangular uniform irradiance to achieve a uniform energy distribution and maximize the contrast ratio of the SLM. After the SLM, the beam passed through various optical components before reaching the resin surface. [32, 33]

Similarly to the system created by Bertsch *et al.* with an LCD dynamic mask, the exposure time was controlled by a shutter that was placed in the beam path and the setup made use of the top-down projection-based SL approach. However, the advantage of using SLM over an LCD as the dynamic mask was the possibility to use a UV light source. Thus, it was possible to utilize the existing wide range of commercial UV-curable resins designed for conventional SL. [33]

This SLM-based method was able to produce components with dimensions in the range of 50 µm to 50 mm with 5 µm sized features. In Fig. 6.1 is presented a double helix structure consisting of 105 layers fabricated using this device. [33]

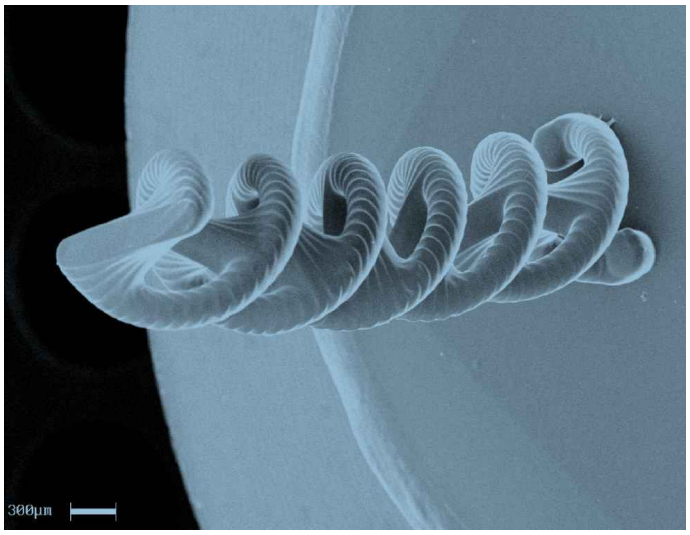

Figure 6.1: A double helix consisting of 50 µm thick layers. Adapted from [33].

6.3 DMD as a dynamic mask

A digital micromirror device (DMD) can be used as a dynamic mask as was done by Sun *et al.* The DMD was illuminated by a UV lamp. The reflected light was shaped according to the defined mask pattern. Then the light passed through a reduction lens. Finally, the image was formed on the resin surface with a reduced feature size. This setup was also a top-down projection-based SL system. [25]

Differently from the approaches making use of LCD and SLM masks, the light does not pass through the mask, but is reflected from the DMD chip. The pixels in the DMD are small and closely spaced (filling factor is 91 %) compared to the LCD and SLM chips. Thus, high resolution and intensity uniformity is achieved. With this DMD-based approach it was possible to fabricate complex 3D microstructures with the smallest feature sizes of 0.6 µm. [25]

7 Research equipment and materials

The objective of this study was to construct a SL-based system that is capable of producing 3D structures with micrometer accuracy and write a program to control the entire process. The projection microstereolithography apparatus (PμSLA) was constructed with do-it-yourself attitude. No construction models were given and the parts used in the setup are either self-made or have been ordered from various Web sites. The resin used in the apparatus is also self-made and the computer programs have been written from scratch.

7.1 Requirements

Achieving micrometer details both in the lateral and vertical direction while manufacturing a part with thin layers and precise shapes is demanding. The lateral resolution depends primarily on the used optics. The area of one pixel at the bottom surface of the resin tank should be around a couple square micrometers to make achieving micrometer resolution possible. The vertical resolution, on the other hand, depends mainly on the resin properties. The curing process should not continue beyond a few micrometers. The exposure time should be optimized to achieve uniform solidification without over-curing. The layer thinness is defined by the movement accuracy of the motorized translation stage. All these properties should be well controlled, which requires suitable software.

7.2 Projection microstereolithography apparatus

In this study, a bottom-up-based PμSLA was constructed for producing structures with a few micrometer accuracy. This section will look into the equipment composition and the working principles. An illustration of the PμSLA is presented in Fig. 7.1.

One of the main components in the setup is a commercial video projector Acer X110, which is based on DLP technology. The original projector lamp acts as the light source. The light is guided through various optical components inside the projector and finally reflected from the digital micromirror device (DMD). The picture is formed by the tiny mirrors in the DMD. The DMD chip contains 480 000 micromirrors, as the native resolution of the projector is 800×600. Each mirror corresponds to a single pixel. By turning a single mirror, the pixel in the image is either black or white. The only alteration made to the projector is the removal of the output lens system. The light intensity distribution shaped according to the desired mask pattern of the DMD is then transferred through a collimating lens,

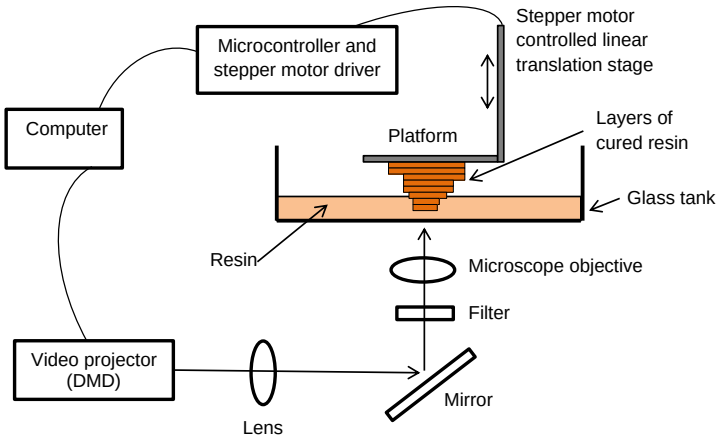

Figure 7.1: An illustration of a bottom-up projection-based microstereolithography apparatus.

mirror, narrow bandpass filter and finally focused onto the bottom surface of the resin vat with a microscope objective. The PμSLA is depicted in Fig. 7.2.

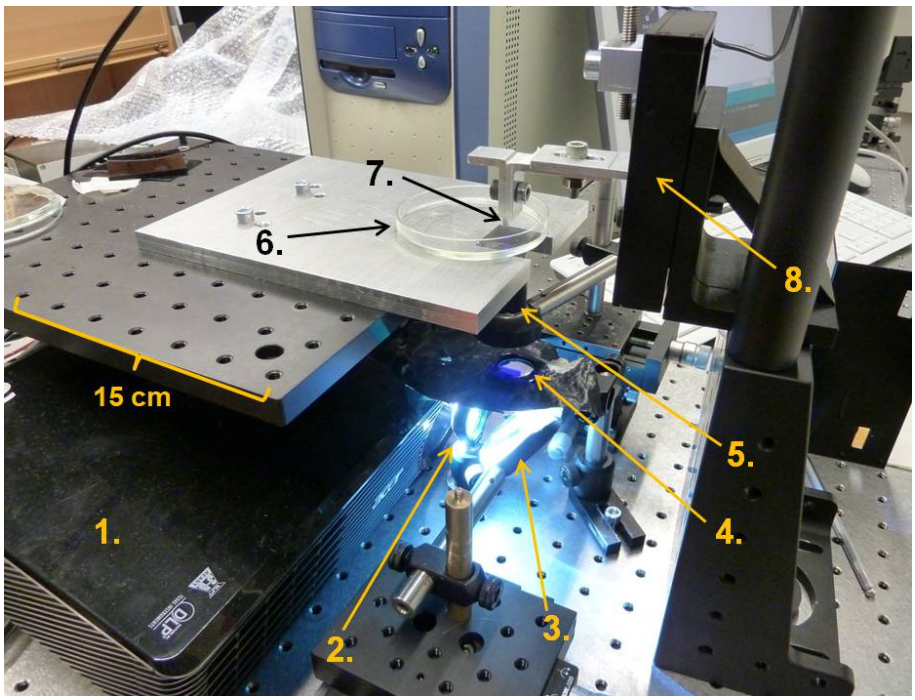

Figure 7.2: The experimental setup for the PμSL process.
1. video projector, 2. collimation lens, 3. mirror, 4. narrow bandpass filter,
5. microscope objective, 6. resin vat, 7. platform, 8. computer controlled elevator.

The collimating lens is required, since the emitted light diverges along the optical axis. The bandpass filter is used to reduce light intensity in order to achieve more accurate control of the curing process. Problems caused by chromatic aberration are

also neglectable, due to the use of narrow-band light. A 420 nm narrow bandpass filter was chosen, since it is the shortest available wavelength (see Fig. 7.3) that has enough energy to keep the exposure times within seconds. The microscope objective focuses the light onto an area of roughly 2 mm^2, which means that one pixel will produce a square of size 2 µm × 2 µm. These numbers can be verified from Fig. 7.4, where the squares are 15×15 pixels and the line between them is 5 pixels wide. Since the distance 1130 µm consists of 580 (29×(15+5)) pixels, the width of one pixel is 1.95 µm. The microscope objective is attached to a vertical translation stage with a micrometer adjuster for controlling the focus point.

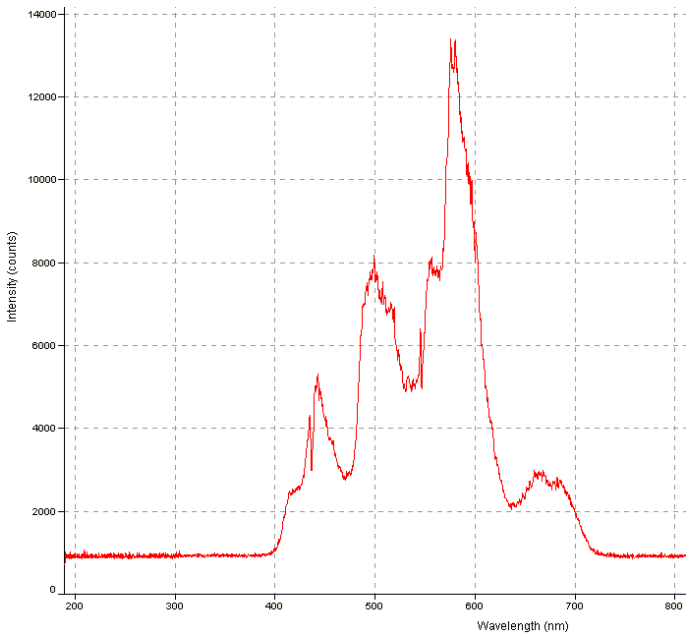

Figure 7.3: The output spectrum of Acer X110 video projector that is reflected from the DMD.

Besides the optical components, a resin vat, an elevator and a computer are required. The resin vat holds the resin and its bottom must be transparent. The vat is made of ordinary glass, but it is coated with Poly(dimethyl siloxane) (PDMS) to reduce the attachment force of the cured resin to the resin vat. PDMS was chosen based on previous experiments, where multiple different coating materials were investigated [34]. PDMS has also been used by other research groups [26]. The elevator is required to move the platform, upon which the part is built on, up and down. In the PµSLA, the elevator is a linear translation stage that is controlled by a stepper motor. A computer is needed for changing the projected image as well as operating the stepper motor. The stepper motor and the image changing methods are presented in more detail in Secs. 7.2.1 and 7.4, respectively.

Before the part manufacturing process starts, the CAD model (in STL format) of the structure is sliced into closely spaced horizontal planes. The sliced planes are stored as bitmap images consisting of black and white pixels. The white areas will

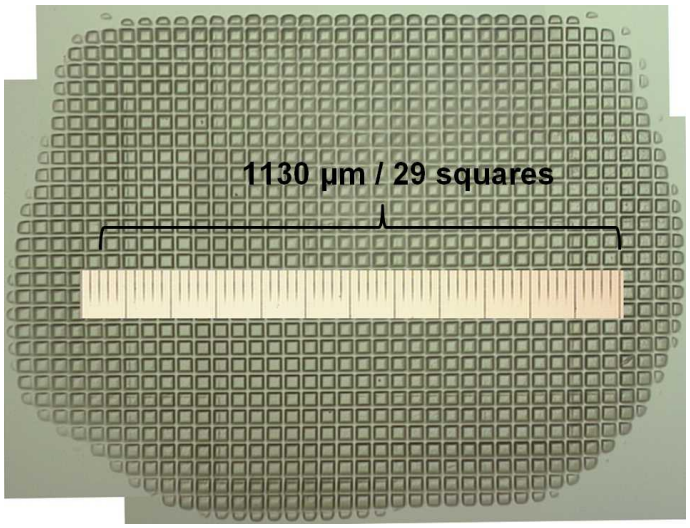

Figure 7.4: An image for confirming the lateral resolution of the PμSLA. The squares are 15×15 pixels and the line between them is 5 pixels wide.

be cured and the dark regions remain liquid. Under one exposure the illuminated areas will all be cured simultaneously. An intensity corrected background image is added to the exposure images, to achieve more uniform curing. The intensity corrected background image takes into account the light intensity hotspots in the light distribution coming from the projector that are caused by various optical components (see Sec. 7.2.2 for more details). These corrected exposure images are placed into one folder and the manufacturing process may start.

To start the process, a small amount of resin is added to the resin vat (the amount of added resin should cover at least the volume of the part to be manufactured, in μSL one droplet is usually sufficient), the video projector is powered up and the outcoming light is blocked with a blocker, so that no light reaches the liquid resin. The platform is lowered so that it barely touches the bottom of the vat. Then the computer program used to control the manufacturing is started. The desired parameter values are entered into the program and the curing process may begin. The program will control both the image projection and the platform movement. First a black image is projected and the blocker is removed. The platform moves up a certain distance and comes back down, but leaves a small gap between the platform and the bottom surface of the resin vat. This gap will define the layer thickness and the size of the gap is determined by the entered parameter values. The platform stops and the image of the first layer is projected. After the exposure a black image is projected again and the platform moves up so that fresh resin may flow under the platform. The platform goes down again, but leaves a small gap between the recently cured layer and the resin vat. Once the platform stops, the image of the next layer will be projected. These steps are repeated until all the images have been delivered and the structure has been manufactured layer-by-layer.

Usually, the first layer has a longer exposure time than the rest of the layers, since the initial lowering of the platform may slightly press the PDMS and the absolute position is unknown. The platform itself may also be slightly tilted in one direction. Thus, to remove these irregularities a thick base layer is cured upon which the rest of the layers are built on.

After the manufacturing process is complete, the platform is lifted out of the resin. The cured structure is rinsed with isopropanol to get rid of excess liquid resin. Finally, the structure can be detached from the platform and the entire process is complete. Excluding the slicing and rinsing processes, the structure manufacturing typically takes between 10 and 60 minutes, depending on the number of layers. One layer is cured every $\backsim$15 seconds.

The PμSLA is inexpensive compared to many other solutions, since the expensive parts, the laser and the scanner system are replaced with a commercial video projector. The current price of the system is between 2 000 - 3 000 €, but with some component optimization the price tag could be lowered to about 1 000 €. The inexpensiveness makes the technology more available to other researchers and organizations, which may lead to new innovations.

7.2.1 Stepper motor and linear movement

A stepper motor is a brushless DC motor that usually has a shaft, which rotates when voltage is applied to the motor terminal. This shaft is then rotated in a stepping manner. The motor can hold the position of the shaft without any feedback sensors, if the motor can handle the applied torque. Each full revolution requires the same amount of steps. Stepper motors are widely used in 3D printers and any solutions involving accurate movement and rotation. Two stepper motors are presented in Fig. 7.5. The geared one is used in the PμSL setup.

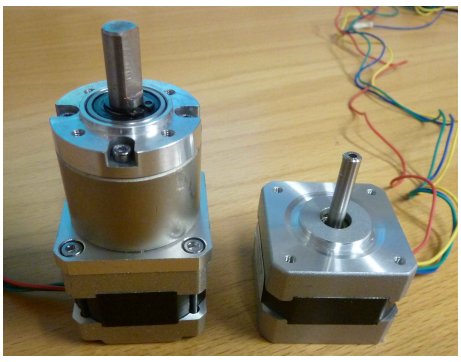

Figure 7.5: Two stepper motors, of which the left one is geared.

Stepper motors can be used to create linear actuators that provide accurate linear motion. The circular motion of a stepper motor can be converted into linear

movement, for instance, via screws and gears. In the PμSLA, the linear motion is achieve by coupling a M6 threaded rod to the stepper motor's shaft and attaching an aluminum block with an internal thread to a linear translation stage as show in Fig. 7.6. The stepper motor is fastened to a fixture to inhibit any rotational or vertical movement. As the shaft rotates the translation stage moves in the vertical direction. To avoid backslash and unwanted movement the coupling of the rod to the stepper motor should be as rigid as possible. So far the self-made coupler has proven to be sufficient, but it may wear out eventually. It may be useful to buy a high quality coupler at some point to get rid of even the smallest backslash.

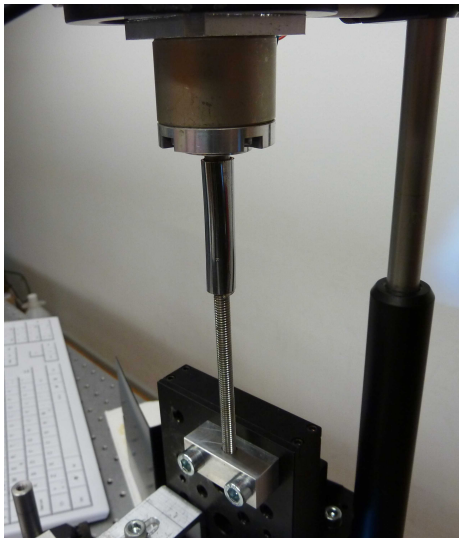

Figure 7.6: A stepper motor coupled to a M6 threaded rod and a linear translation stage.

The pitch of the screw rod attached to the stepper motor shaft has a significant role in determining the linear movement accuracy. The smaller the pitch the more the shaft has to rotate to achieve a set distance. The pitch of a M6 thread is 1 mm. Therefore, one full revolution will result in 1 mm vertical movement of the translation stage. For instance, the step distance is 5 μm/step, if a 200-step stepper motor is coupled with a M6 thread. However, the step angle accuracy is around 5 % of a step. Thus, the actual distance of one step may slightly deviate from 5 μm.

In the PμSLA the platform is moved by using a geared stepper motor with a 13.73 gearbox attached to a 200-step stepper motor. Thus, 2746 (13.73×200) steps are required in order to go one full revolution. For a M6 threaded rod this translates to a movement of 0,364 μm/step. Therefore, the step size accuracy meets the 1 μm step size requirement of PμSLA, even taking the step angle error of ±5 % into account [35].

7.2.2 Hotspot compensation

The intensity of the reflected light from the DMD is not evenly distributed across the exposure area. This may be caused by the properties of the light source and various optical components (lenses, waveguides etc.) in the DLP projector. The output image of a uniform gray object is presented in Fig. 7.7. The nonuniform exposure can be clearly seen from Fig. 7.8, where a single layer of multiple small squares has been cured. The Figs. 7.7 and 7.8 show the location of the high intensity areas to be quite the same in both figures.

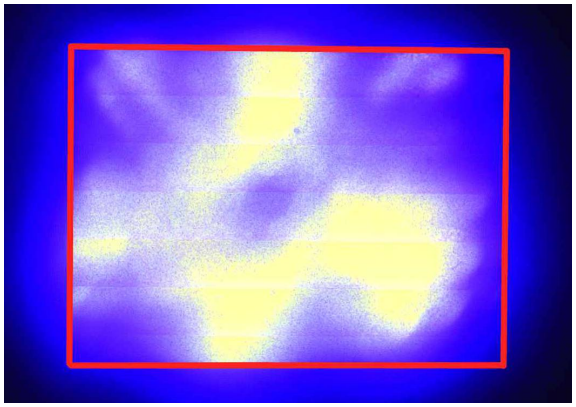

Figure 7.7: The output image of the projector at the bottom surface of the resin vat. The image formed from the DMD is inside the red lines.

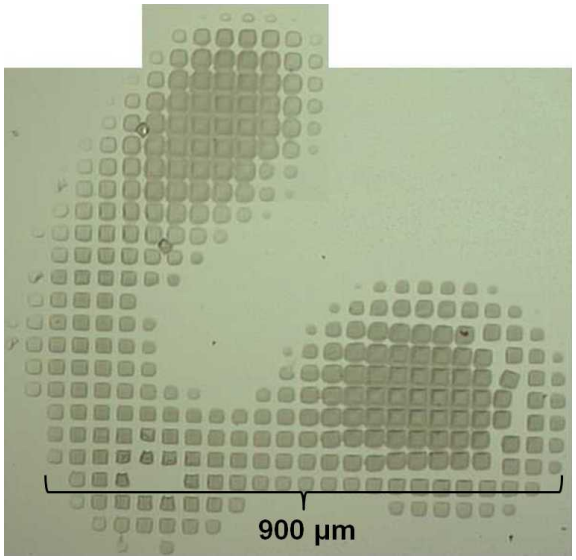

Figure 7.8: Curing one single layer consisting of small squares presents the problem with hotspots. In two areas the squares have been combined due to high intensity, while the top right corner is below the curing threshold.

The hotspots can be compensated for by combining the images, with an intensity corrected background image. The intensity corrected background image is a

grayscale image that evens out the intensity differences between the different areas.

The background image can be achieved by at least three adequate methods. First, one can use an intensity meter to measure the intensity of small areas individually and then use the collected data to form a corrected background image. This method is troublesome without a proper intensity meter, since the entire lit area is only around 2 mm^2. One has to measure extremely small areas if the image would be constructed from a large number of data points. The more data points are gathered, the better the compensation image will be. One may investigate the intensity of a single small area by only lighting up the selected area. This can be easily done by projecting a black object with a white dot in the investigated area. Changing the position of the white dot, one can measure the intensity of each separate area. However, this method does not take into account how the intensity of a specific area is affected by other bright areas. It is possible that the areas outside the measuring spot result in an intensity rise at the spot being measured. Thus, a better image correction might be achieved by investigating a fully lit output.

This intensity measurement method was briefly tested. The image area was divided into 48 pieces, 100×100 pixels each. The intensities of these areas were measured independently. The measurement results are presented in Table 1.

Table 1: Intensities ($\mu W/cm^2$) at different parts of the output image

26	45	70	106	91	54	37	21
30	58	85	102	78	53	41	24
42	67	81	69	66	74	61	33
48	69	79	73	85	98	82	38
38	55	80	85	76	82	67	27
19	33	59	63	46	43	31	13

The intensities vary between 13 and 106 $\mu W/cm^2$. The outermost values deviate so much from the middle area ones that it is not sensible to try to achieve complete compensation over the entire area. It would lead to a very dark image with white edges, which would increase the exposure time for curing one layer dramatically. The outer areas are dark mostly due to the microscope objective. The entrance to the objective is slightly smaller than the collimated light beam from the projector, thus the edges will not be shown properly. Due to this limitation, it was decided to use only the central parts of the image area for 3D part manufacturing. Besides, most sliced cross-section images will not extend to the outer edges and even if they did, they could be resized with the operation program, which is presented in Sec. 7.4.2.

A target intensity value is set and all the investigated squares should reach the same value. Based on the values in Table 1 and neglecting the outermost values, the target can be set to 50 $\mu W/cm^2$. Then all the brighter areas are made darker until they meet this target value. Combining all the compensated areas will result in an intensity compensated background image. The result is presented in Fig. 7.9.

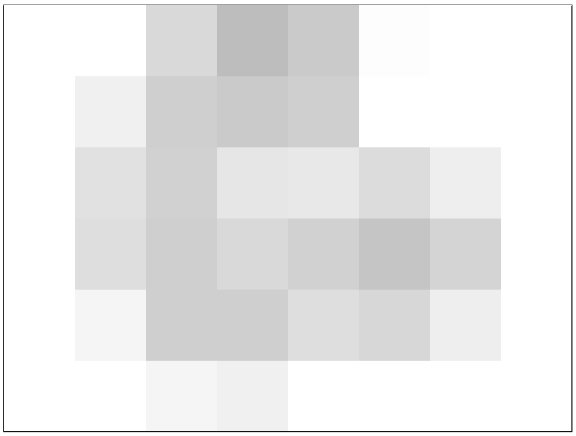

Figure 7.9: The intensity corrected background image achieved using an intensity meter.

The advantage of this method is that the actual output intensities of different small squares are closely even. However, as shown in Fig. 7.9, the separate squares are large and the intensity within the squares may greatly vary. Thus, the area of a single square should be greatly diminished to increase the resolution, but it will lead to a huge number of measurements at very low intensity values.

A second way to construct a compensation image is to take a photograph of the image shown at the bottom surface of the resin tank and use it to construct an intensity corrected background image. A photograph of the output is shown in Fig. 7.7. The actual image area inside the red lines is extracted and loaded into an image manipulation program. The loaded object is made black and white after which the colors are inverted. The result is shown in Fig. 7.10.

Although the image has high resolution and the shapes of the bright areas in Fig. 7.7 are followed accurately, the grayscale levels are most likely incorrect. The right brightness of the image must be investigated through trial and error. The photograph used in the image conversion process may also be erroneous, since the brightest areas seem to have the same intensity value (the same applies for the darkest areas).

The third option to create an intensity corrected background image is to cure 2D chessboards. In this context, the 2D means that only one single layer has been made. By curing a single layer and observing how well each part of the image has been cured, one may adjust the background image accordingly. Adjusting the grayscale values is simpler if the whole image area is divided into squares that are

Figure 7.10: The intensity corrected background image achieved using a photograph of the output at the bottom surface of the resin vat.

adjusted separately. Thus, using the chessboard approach, the background image can be produced by iterating the curing process. The starting image is shown in Fig. 7.11 along with the curing result achieved with it.

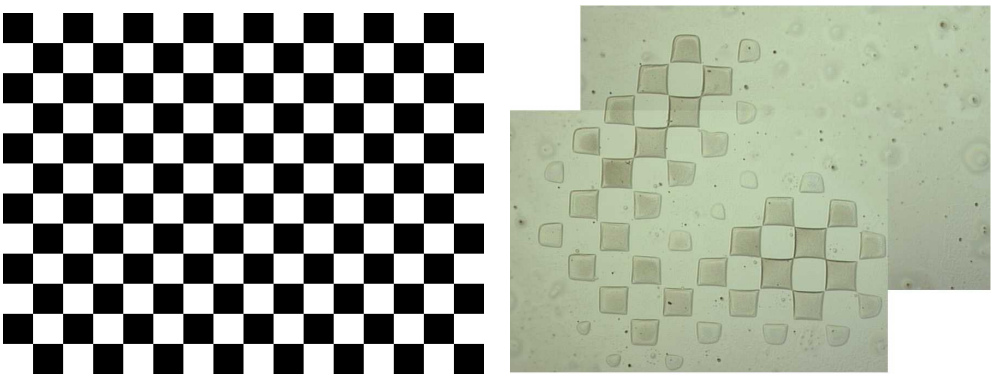

(a) The projection image. (b) The curing result.

Figure 7.11: Curing result of a single layered chessboard, using the image shown in (a).

The areas cured in Fig. 7.11(b) should have their corresponding squares in the projection image made darker so that the curing would be more uniform. After repeating the adjustment process multiple times one obtains an intensity corrected chessboard. The result is shown in Fig. 7.12.

The difference between not using and using an intensity corrected background image is clear by comparing Figs. 7.11(b) and 7.12(b). Even though some of the squares have got displaced in Fig. 7.12(b), due to the washing method used to remove the excess liquid resin, the squares in 7.12(b) are more identical than the squares in Fig. 7.11(b). However, only half of the image area is intensity corrected. One has to do the same iteration for the color inverted chessboard, i.e., inverting the colors in

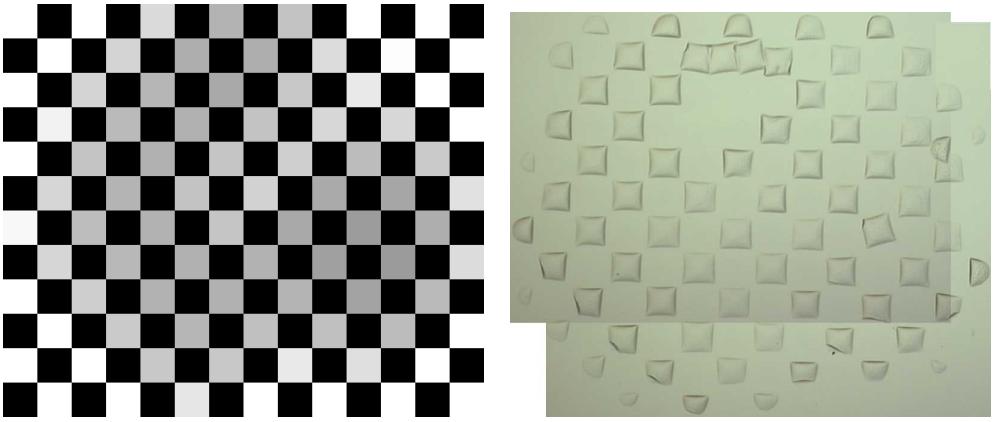

(a) The corrected projection image. (b) The curing result.

Figure 7.12: Curing result of a single layered chessboard, using the intensity corrected image shown in (a).

Fig. 7.11(a). Combining the correction images will result in the actual background image that can be used in future processes. The intensity corrected background image is shown in Fig. 7.13 along with an array of cured small squares.

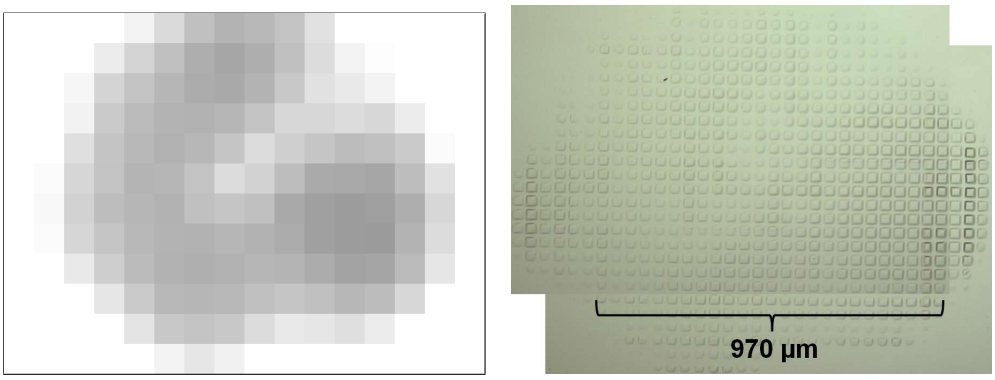

(a) The intensity corrected background image. (b) The curing result using the same projection image as in Fig. 7.8.

Figure 7.13: Curing result using an intensity corrected background image.

Comparing Figs. 7.8 and 7.13(b) one can notice the dramatic effect of intensity correction. Nearly all the squares are visible in Fig. 7.13(b) and the squares have not merged at any point.

In summary, three different intensity correction methods were briefly investigated and three background images were achieved, Figs. 7.9, 7.10 and 7.13(a). In all three the darkened area has a similar shape. Thus, the locations of the hotspots have been verified.

The background image achieved using an intensity meter consists of too large

areas to be useful, more measurements should have been executed to reach an adequate result. The problem with the image made through the image manipulation is the brightness adjustments. Therefore, the intensity corrected background image used in the further processes was chosen to be the one in Fig. 7.13(a).

Hotspots are not always an issue that needs to be dealt with in PSL. Instead of using a commercial video projector, one may use a lamp, collimating lens set, DMD and a lens tube, to achieve uniform light intensity as done in a PμSL process developed by Ha *et al.* [27]

7.3 Resin

In this study, two different resins, one with long and one with short penetration depth, were used to test the apparatus performance. The resin with long penetration depth consists of trimethylolpropane trimethacrylate (monomer), Lucirin TPO-L (photoinitiator) and 4-phenylazophenol 98 % (neutral absorber). The composition of the resin with short penetration depth consists of the same monomer and photoinitiator, but the neutral absorber is Disperse orange 13. These compositions were chosen based on previous research [36]. The resin with Disperse orange 13, was also successfully used in manufacturing structures with 10 μm resolution in earlier experiments. While the resin with short penetration depth is adequate for μSL, the long penetration depth resin can be used to investigate the operation principle more easily. [36]

In general the fabrication process is easier with long penetration depth resins. With short penetration depth resins the distance between the platform and the resin vat must be extremely short, since the gap must be smaller than the maximum curing depth of the resin. Too large a gap will immediately ruin the entire manufacturing process. Positioning the platform close to the bottom surface of the resin vat is not simple, if the resin vat is coated with a soft material and there are no designed equipment for measuring the distance between the platform and resin vat. The platform surface area should also be in relation with the curing area. It is possible that a layer of resin with unknown thickness gets trapped between the platform and the bottom surface of the resin vat when the platform is lowered all the way down. This issue is briefly discussed in Chap. 8. Thus, using a long penetration depth resin the curing of the base layer is simpler and the layer thickness accuracy of the following layers does not have to be so high. Therefore, the first curing experiments are usually conducted with long penetration depth resin.

7.4 Software

The software used in the part fabrication process should be able to handle three different tasks. First, the CAD model of the piece to be manufactured will be sliced and converted into black and white images, with possible grayscale alteration. Second, the microcontroller must accept input values sent from the computer and move the stepper motor accordingly. Third, a computer program is required to control the image projection (exposure time and image changing) synchronized with the movements of the stepper motor. The computer program should accept at least the following parameters: exposure time, delay (before and after each layer has been manufactured), image size, motor movement speed and layer thickness.

The image projection and changing operate in the same way as projection of slides in slideshow software. First a picture is presented, then there is a transition followed by a new image. The video projector is connected to the computer via a VGA cable and the same image will be shown in both devices. Thus, the idea is to have a slideshow program, which is synchronized with the motor movements, to control the image projection.

7.4.1 Slicing and preparing images

In this project the slicing of an STL file was done using Freesteel Z-level slicer. It is a free to use command-line utility used for slicing STL files. The slicer has multiple options for controlling the slicing. For instance, the output file type, size, resolution, color, layer thickness and the amount of slices can be chosen with ease. An example of the use of the Freesteel slicer is presented below.

Slicing an STL file, in this example case winnerscup.stl, is done in the following manner with the Z-level slicer. First, the 3D model of the object must be in upright position, in other words, the bottom of the object must be in the xy-plane and the object should be grown in the same direction as the positive z-axis. If this is not the case, the STL file must be rotated with a CAD program to meet the above requirements. Otherwise the object will be sliced in the original orientation and it will be manufactured accordingly, which may result in the part to be manufactured sideways or upside down. Manufacturing the object upside down might be acceptable in some cases, but the manufacturing may also be impossible if the top part of the object is pointed and there are no supporting structures. Second, the STL file is placed in the same folder as the slicer program. Third, command-line is started and "slice" command is run. The file winnerscup.stl can be sliced by typing the following in the command-line:

slice -r0.0001 –layer=0.01 –core=white –cavity=black –width=800 –height=600
c:\STL\winnerscup.stl -z0,70,1 -o cup.png

The first parameter is the tool radius. The smaller the radius the smaller details will be distinguishable. The second one is layer thickness that is used to slice the structure horizontally. The core and cavity parameters affect the color of the output image. In PSL the image should be white on the area that is cured and rest of the image should be black. The image resolution can be adjusted by altering the width and height parameters. The structure size and the amount of slices are set in the second to last parameter. The first numerical value after "-z" stands for the starting position and the second one for the stopping position. The ending position is set to 70, since the winnerscup.stl structure is known to be 70 units high (can be confirmed with a CAD program). The final number controls the slicing frequency. The value 1 will result in 70 slices, while 0.5 would result in 140 slices. The final option is used to define the file type and name of the output images. Each slice will be saved as an image for further processing. A 3D model of the winnerscup.stl and three example images from the slicing process are presented in Fig. 7.14.

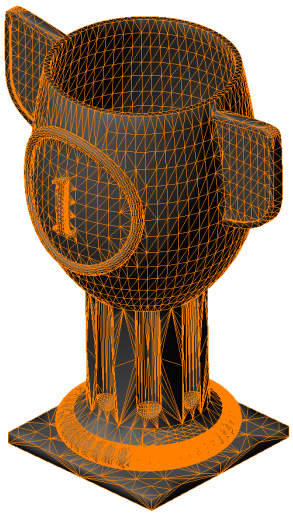

(a) CAD model in STL format.

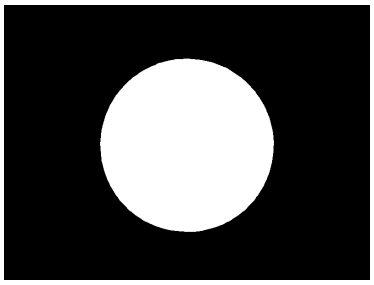

(b) Image of layer 5/70.

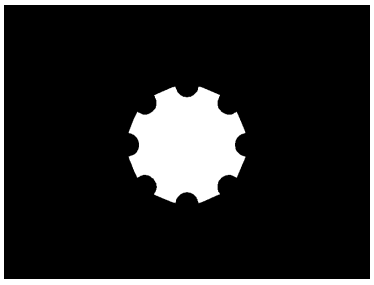

(c) Image of layer 21/70.

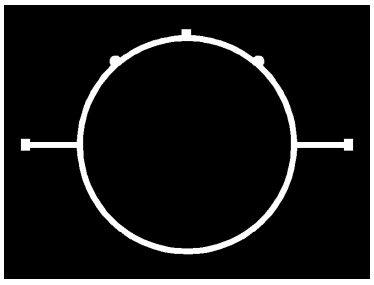

(d) Image of layer 52/70.

Figure 7.14: A CAD model of winnerscup.stl and three images sliced from it.

Once the STL model has been turned into images, the intensity corrected background is applied to them. This is done in two steps. First, the white areas in

the images are made transparent. Second, the images consisting of transparent and black areas are separately placed upon the intensity corrected background image. Due to the possibly high number of images achieved from the slicing processes, these two conversion processes should be applied to all the images simultaneously. One way to do this is to use a freeware image processing system "GraphicsMagick". The main advantage of GraphicsMagick is that it can be operated using a command-line utility in Linux environment. The images are processed in the following manner. First, all the black and white images are placed into the folder where GraphicsMagick is installed. Second, the following command is executed:

./gm mogrify -transparent white *.png

This will make all the white areas transparent. Third, the background image is placed into the same folder with the rest of the images. Fourth, the following command is executed:

for infile in cup*.png; do outfile=‘echo $infile | sed -e ’s/image/result/ ; s/\..*//’‘.png; ./gm composite $infile background.png $outfile; done

This will make all the images that start with the letters "cup" to be individually composed with background.png, which in this case is presented in Fig. 7.13(a). Thus, all the images will include the hotspot compensation. The result is presented in Fig. 7.15 for the same images as in Fig. 7.14.

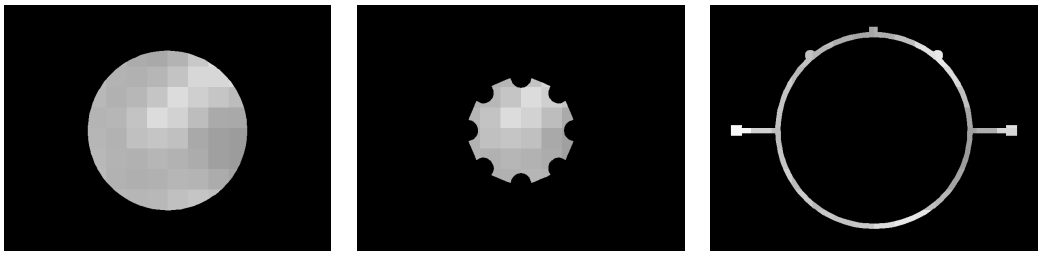

(a) Image of layer 5/70. (b) Image of layer 21/70. (c) Image of layer 52/70.

Figure 7.15: Three images with intensity corrected background (compare with images in Fig. 7.14).

7.4.2 Operation program

Two different programs are needed for operating the manufacturing process. One program is uploaded to the microcontroller for controlling the stepper motor and one is used to display the sliced images and adjust the operation parameters such as exposure time.

The stepper motor is controlled using an Arduino Uno microcontroller and Easy-

Driver stepper motor driver. The connection of the components is shown in Fig. 7.16. The EasyDriver breaks down the steps of the stepper motor into microsteps. Eight microsteps equal one step. Thus, a 200 step stepper motor will make a full rotation with 1600 microsteps. Microstepping makes the rotation smoother, but does not necessarily increase stepping accuracy, because increasing the number of microsteps causes the incremental torque per microstep to drop significantly [37].

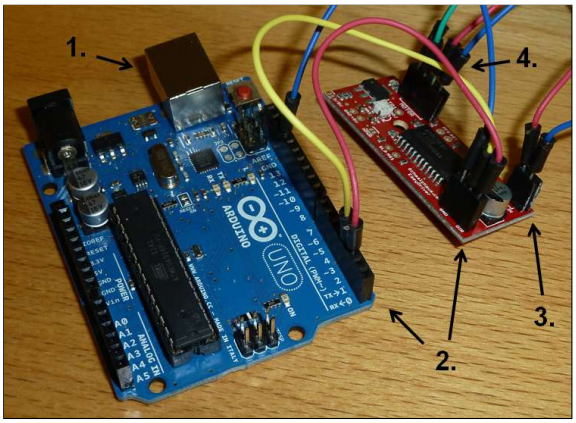

Figure 7.16: The connections between a computer, Arduino Uno and EasyDriver. 1. USB-B port for computer connection, 2. DIR and STEP pins, for communication between the microcontroller and stepper motor driver, 3. connection to a power supply, 4. stepper motor connection.

The program uploaded to Arduino Uno controls the motor movement according to the data received via a serial port. The uploaded code with detailed explanations can be found in Appendix A.1. The flowchart of the program is presented in Fig. 7.17. Once the program has been uploaded it will stay in the microcontroller's memory until a new program is uploaded.

The program for controlling the slideshow and giving commands to the microcontroller was written in Python. Some methods used in the program were inspired by the book *Sulautetut*, written by Tero and Kimmo Karvinen [38]. The graphical user interface (GUI) of the program is presented in Fig. 7.18.

Exposure time, delay and movement can be controlled by typing the desired values into the three empty cells using natural numbers. The size of the image, motor speed and layer thickness can be chosen by using the radio buttons.

The four buttons at the bottom of the GUI are used to move the platform in a stepping manner. The platform can be moved in 5 µm and 200 µm steps up or down. This is useful at the start of the manufacturing process, since the platform has to be lowered so that it barely touches the bottom surface of the resin vat. After the entire structure has been manufactured, the platform can be raised from the resin by using the same buttons or pressing the Page Up key on the keyboard.

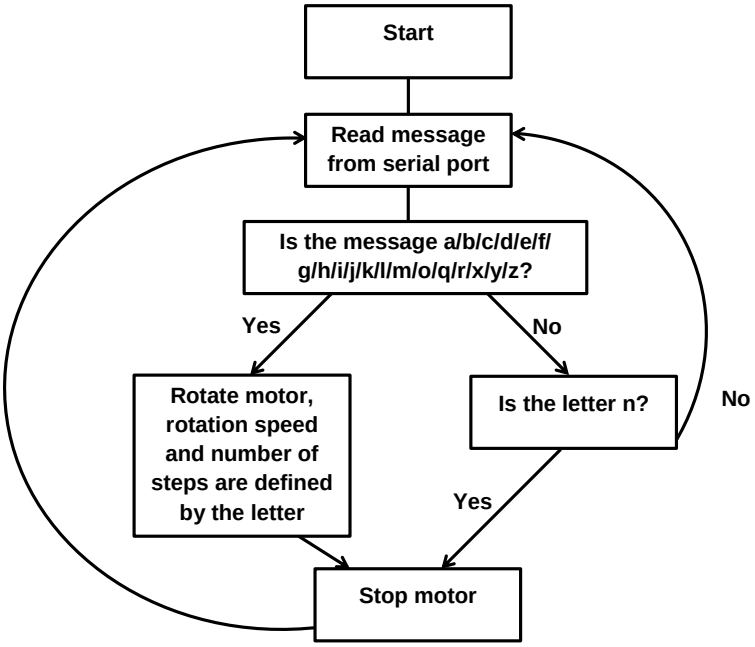

Figure 7.17: Flowchart of the program uploaded to Arduino Uno.

The program is started by pressing the wide button in the middle and then pressing the s key on the keyboard. Once the wide button is pressed the screen becomes black. The actual manufacturing process will not start until the s key is pressed. Before the s key is pressed the user must remove the blocker in front of the projector and the removal should be done while the screen is black.

Once all the layers have been cured, the screen will remain black until interrupted by the user. Using the Page Up key one can lift up the platform before exiting the program. Pressing the Esc key will shut down the entire program, after which it has to be restarted for the next manufacturing process.

The source code of the program with detailed explanations can be found in Appendix A.2. The flowchart of the program is presented in Fig. 7.19.

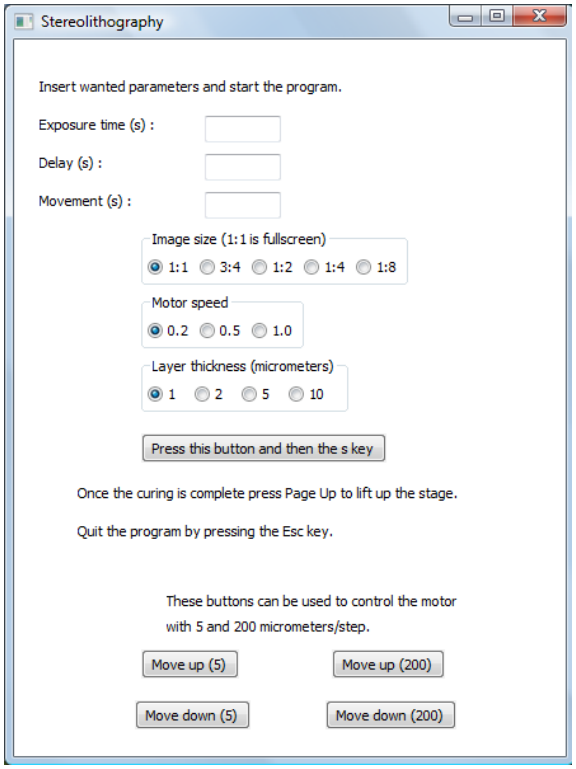

Figure 7.18: The graphical user interface (GUI) of the computer program controlling the PμSLA.

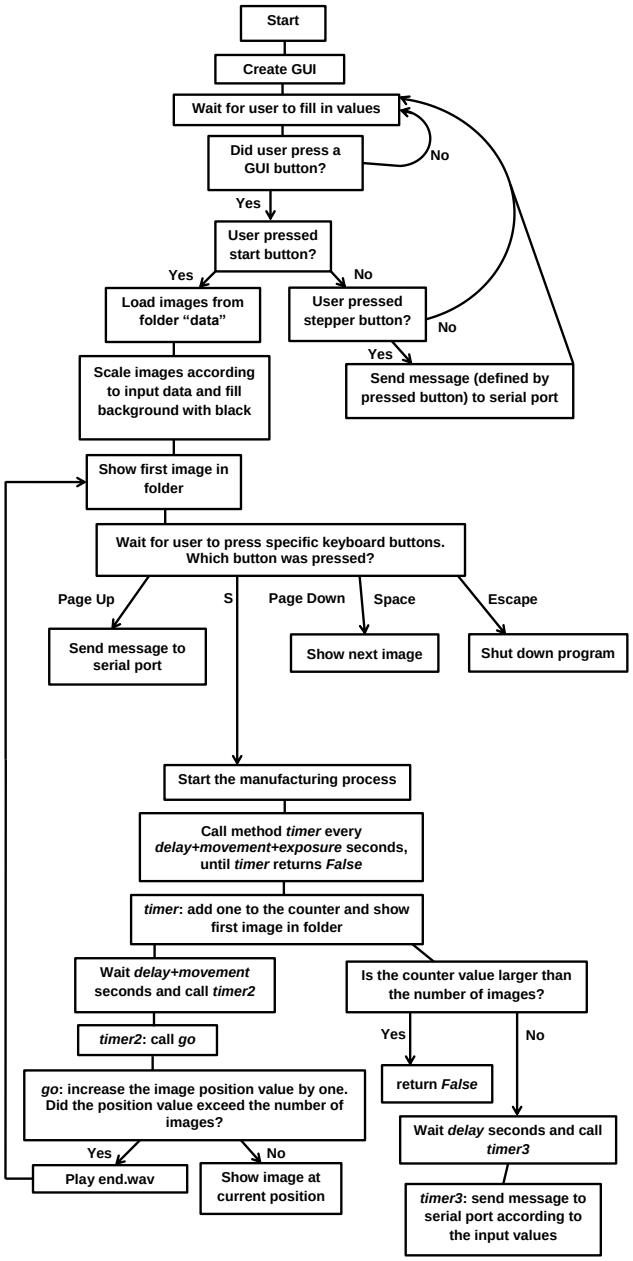

Figure 7.19: Flowchart of the program used for controlling the slideshow and giving commands to the Arduino Uno microcontroller.

8 Results

The goal in this thesis work was to construct a PμSL system that can be used to fabricate structures with micrometer-sized features. One important factor of the manufacturing process is the performance of the written computer program. For 3D part manufacturing to be possible the slideshow and the z-motor must be properly synchronized. If an image is projected while the motor is still moving, the fabricated structure will be ruined. The program should project images only when the motor is standing still and there is a new layer of fresh resin between the resin vat and the platform.

The movement accuracy of the motorized translation stage must be better than one μm. The motor movement accuracy as well as the performance of the computer program were tested by curing multiple squares of different sizes upon each other. Thus, it is possible to investigate whether the platform movement corresponds to the input values set into the program and the manufacturing concept is adequate.

For testing the operation performance, two different resins, one with long and one with short penetration depth, were used as discussed in Sec. 7.3. The one with long penetration depth was used for testing the operation principle, while the short penetration depth resin was used to fabricate high-detail structures.

The result of fabricating a 30 layered structure using a long penetration depth resin is presented in Fig. 8.1. The structure consists of a base layer and three different sized squares. After the base layer there are 212×212 pixel squares followed by 150×150 and 100×100 pixel squares. Each square contains 10 layers. The layer thickness was set to 10 μm.

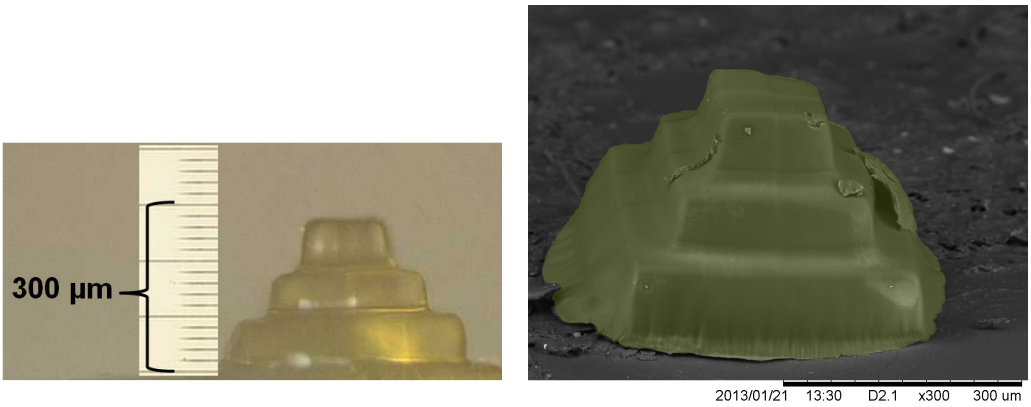

(a) An optical microscope image. (b) A SEM image.

Figure 8.1: A structure consisting of 30 layers that are 10 μm thick.

From Fig. 8.1 one can verify that the layer thickness corresponds quite well to

the set value of 10 µm. Thus, the platform movement and the program used to control the fabrication process operate commendably. However, it is clear that the fabrication accuracy of the part is not close to a few micrometers. The edges of the squares are round and the entire structure looks blurry. The reason is most likely bad focusing and unoptimized exposure time. However, the manufacturing of the structure served its purpose and demonstrated that the computer program operates well together with the stepper motor.

Switching to a short penetration depth resin for fabricating high-detail objects both in the vertical and horizontal direction proved to be difficult. The same type of manufacturing method was used as with the long penetration depth resin, but the accuracy never seemed to be sufficient. The structure in Fig. 8.2 consists of 30 layers similarly to the structure in Fig. 8.1, but the layer thickness was lowered to 5 µm. The structure is deformed and not all of the layers are visible.

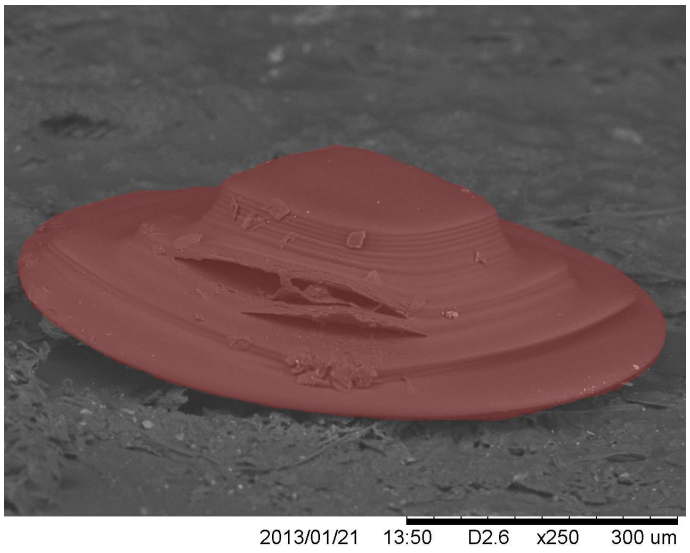

Figure 8.2: A SEM image of a structure consisting of 30 layers that are 5 µm thick.

By simply comparing the two structures, fabricated using the same focus point but different resins, the dissimilarity is clear. The images of the structures from above are presented in Fig. 8.3. They both consist of similar square-shaped layers stacked upon each other as in the previously presented structures. Even though the projection images are the same in both structures, the structure fabricated using the short penetration depth resin seems smaller and distorted. The structure in Fig. 8.3(a) consists of accurate squares as it should. Changing the resin significantly affected the curing result. However, the drop in curing accuracy is not solely explained with the use of a different neutral absorber. The exposure time was also increased for the short penetration depth resin as it will be discussed in more detail in Chap. 9.

As mentioned in Sec. 7.3 the platform size may affect the curing result. The

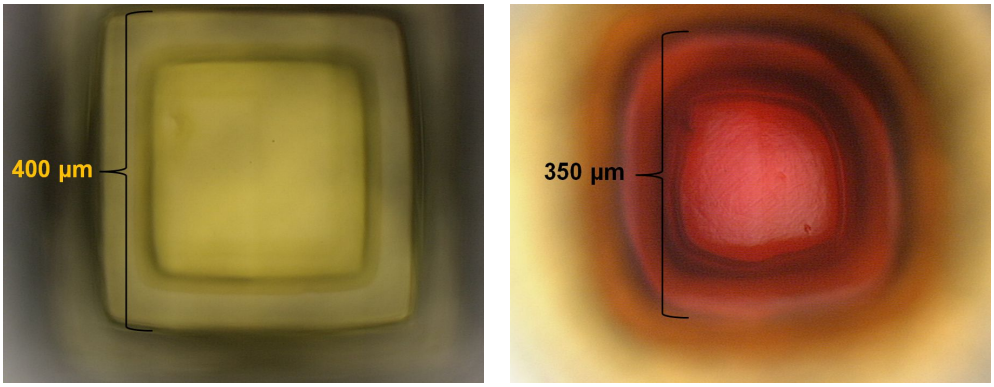

(a) Long penetration depth resin. (b) Short penetration depth resin.

Figure 8.3: Two structures fabricated with different resins, but using the same projection images and focus points. The structures are viewed from above.

same structure was manufactured with two different-sized platforms in Fig. 8.4. Both structures were fabricated using the same manufacturing parameters, only the platform was changed. The area of the large platform was about 8 mm^2 and the small platform was roughly 13 times smaller (0.6 mm^2). The issue with the structure in Fig. 8.4(a) is that the lowest 10 layers are much thicker than they should be and the final 20 layers are thinner than they should be. On the other hand, in Fig. 8.4(a) the thicknesses of the three sets of layers are balanced.

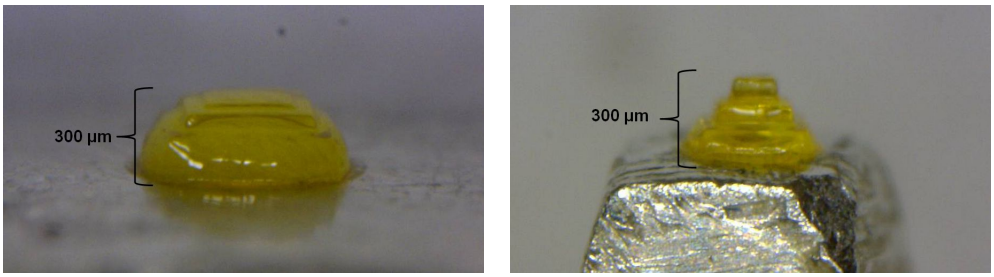

(a) Using a large platform, area of platform $\backsim$8 mm^2.

(b) Using a small platform, area of platform $\backsim$0.6 mm^2.

Figure 8.4: Two structures fabricated with same parameters, but using different-sized platforms.

Due to these remarkable difficulties in fabricating a stack of squares using the short penetration depth resin, the manufacturing of fine-detail 3D models with overhanging structures were postponed. However, the PµSLA has been previously used successfully to manufacture fine-detail structures with less than 10 µm thick overhanging bars. Some previously manufactured objects are presented in Fig. 8.5. Based on the structures in Fig. 8.5 it is evident that the short penetration depth resin is adequate for PµSL, since the vertical resolution is higher than 10 µm.

The issues mentioned in this section are discussed in more detail in Chap. 9. The

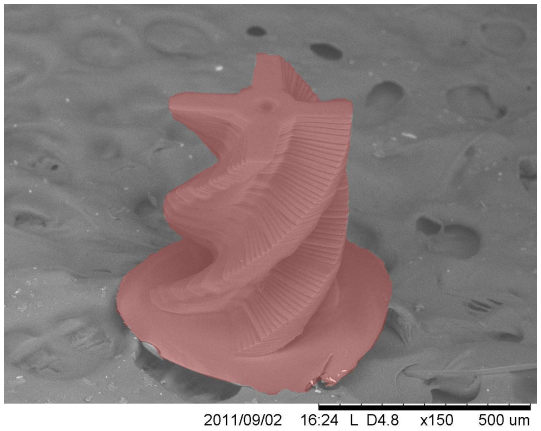

(a) A propeller-looking stucture. Each layer is 10 µm thick.

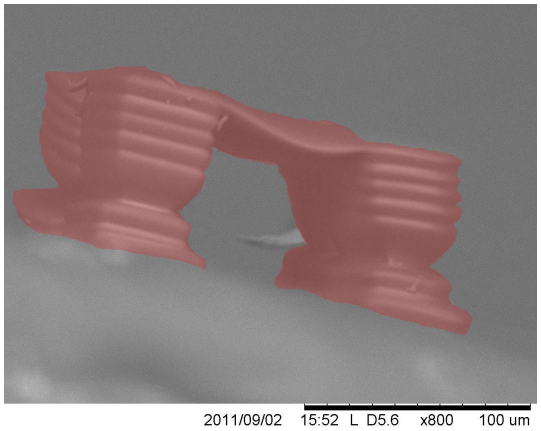

(b) An overhanging roof on four pillars.

Figure 8.5: Fine-detail structures that were fabricated in previous research experiments.

main issue is the loss in accuracy when the resin was changed to a short penetration depth one.

9 Summary and conclusions

The purpose of this study was to construct a PμSL device and write a computer program for controlling the manufacturing process of three-dimensional objects. The hardware of the PμSLA consists of a video projector, various optical components, resin vat, platform, a linear translator connected to a stepper motor and a computer.

The written software consists of two parts. One program was uploaded to an Arduino Uno microcontroller to operate a stepper motor based on the commands received via a serial port. The second one was used to control the fabrication process and send movement commands to the microcontroller. The computer program takes as input all the parameters related to the manufacturing process, such as exposure time, layer thickness and motor movement speed.

The program operated adequately, no issues were caused by the motor control or the image projection. This was confirmed by fabricating a structure consisting of a stack of squares with different sizes, see Fig. 8.1. The lateral resolution also met the objective. The size of one pixel at the bottom of the resin vat is 2 μm × 2 μm, as verified from Fig. 7.4. Thus, the operation principle and projection accuracy met the set goal.

The disappointing part of the PμSL system was the fabrication performance when a short penetration depth resin was used. The shape of the structures was blurry (Fig. 8.2) and the accuracy was far from what had been achieved in previous short penetration depth resin experiments (Fig. 8.5). There are a few major issues that most likely caused the problems.

The things that were changed compared to the equipment used in 2011 were the operation program, resin vat, microscope objective, intensity compensation and probably the properties of the resin. The reason for the poor fabrication result should be found from these factors.

Previously the fabrication process was performed using two independent programs that were not synchronized with each other. One program moved the stage at regular intervals and the other was a simple slideshow program that changed the image at regular intervals. The current program is more suitable since it prevents the slideshow and the stage movement from getting out of synchronization, which occurred with the previous system after about every 20 layers, if counter measures were not taken.

One problem with the current setup seems to be the coating material used in the resin vat. The exposure time was increased when the resin was switched to the short penetration depth one, which seemed to lead to difficulties.

As the exposure time is increased, the attachment force between the bottom of the resin vat and the cured resin layer increases [34]. This sticking may be so powerful that it rips off pieces of the soft PDMS every time a layer is cured and the platform is moved away. This ripping may be observed from Fig. 9.1, where a pit has been left behind on the PDMS after every fabrication process. However, such pits did not form when the long penetration depth resin was used, since the exposure time was shorter. With the long penetration depth resin the exposure time for the base layer was 5 seconds and for the rest of the layers 3 seconds, while for the short penetration depth resin the exposure times were 20 and 6 seconds, respectively. A shorter exposure time at the base curing led to a fabrication failure, since the first layer would not stick properly to the platform. However, using a long exposure time exerts stress to the PDMS coating. Once a small pit has formed in the PDMS, the following layers are affected by the pit and the shape accuracy may be lost or the shape of the pit itself will be cured onto the structure, as in Fig. 9.2.

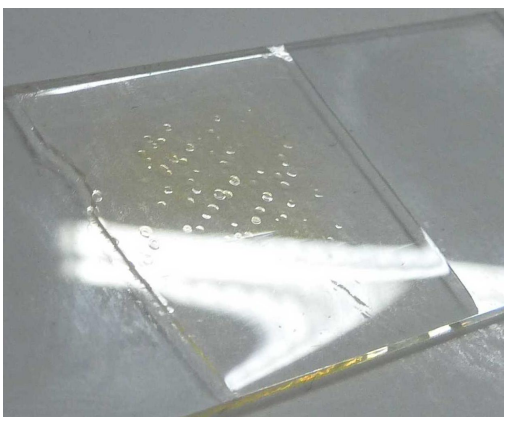

(a) A microscope slide with a PDMS coating. Small pits caused by the ripping force between the cured resin layer and PDMS are visible.

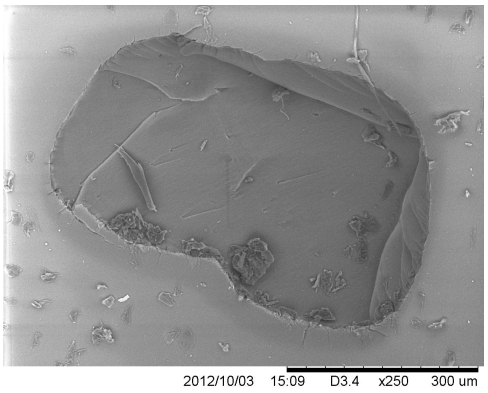

(b) A SEM image of a pit.

Figure 9.1: Pits caused by the cured resin ripping off from the PDMS surface.

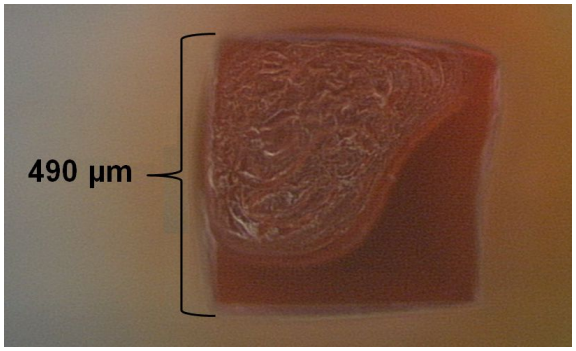

Figure 9.2: A significant defect due to poor mechanical strength of PDMS and long exposure times.

The problem of ripping off parts of PDMS was investigated in a previous study and the ripping effect was reduced by using a thicker layer of PDMS [34]. Thus, the resin vat was changed to a petri dish with a thick layer (>2 mm), see Fig. 9.3. However, this produced new issues, because the bottom of the petri dish is not completely flat. The bottom is slightly convex, which is a problem when the depth of focus is short. Small changes in the position of the dish will lead to unfocused curing. Thus, product fabrication was difficult and often the base layer was not cured despite multiple attempts. Sometimes the process worked and sometimes it did not, which made parameter optimization tests challenging, since one had to guess whether the changed parameter affected the result or was it just irregularity in the fabrication process. Also the advantages of a thick PDMS coating were previously only tested with a long penetration depth resin [34].

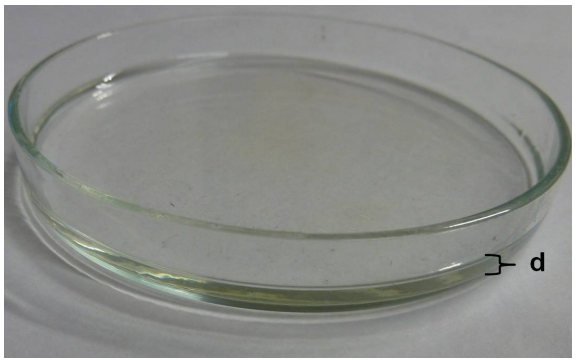

Figure 9.3: A petri dish with a thick coating of PDMS, d >2 mm.

The microscope objective was changed from one with a magnification of 20 to one with 15. Also the working distance got about 10 times longer, which is useful when a thick resin vat coating is used. The working distance limits the possible thickness of the coating. The lateral resolution decreased in the change, due to the drop in magnification, which also lowered the light intensity and thus increased the exposure time.

The intensity compensated background image was applied to all the projected images to even out the intensity differences across the light source and to make the curing more uniform. This seemed to work well as shown in Sec. 7.2.2. While it evens out the intensity differences it also increases the exposure time, since the overall light intensity is reduced. The intensity corrected background should also be more detailed than the one presented in Fig. 7.13(a), since the transitions between the intensity corrected squares are dramatic. This can be observed from Fig. 8.1(b), where the top part of the structure seems to consist of four separate squares. The edges of the intensity corrected squares should be slightly blurred to avoid this defect.

It may also be possible to directly affect the homogeneity of the exposure. Sun *et al.* [25] introduced a fly-eye type optical homogenizer at the lamp output. Thus, a uniform illumination on the DMD chip was attained. The intensity variation

was within ±5 %. The intensity uniformity might also be video projector related. Higher quality optical components in the projector may reduce the forming of hotspots.

The short penetration depth resin used in this study was from a more than one year old batch, which may affect the curing properties. The resin had also nearly run out and only the bottom precipitate was left. This may be one factor affecting the curing accuracy. Thus, a new batch should be made for future experiments.

The size of the platform should be chosen carefully as observed from Fig. 8.4. Basically, the smaller the better, since the moment when the middle part of the platform touches the resin vat can be determined more reliably when the platform is lowered into the resin at the start of the fabrication process. The smaller the platform is, the less resin can be trapped beneath the platform. However, the area of the platform should be large enough to ensure sufficient attachment of the base layer to the platform. Currently, there is no method for controlling the absolute position of the platform. Thus, the platform is always lowered carefully to touch the PDMS coating in the resin vat every time at the beginning of the manufacturing process. A measuring device for the absolute position may ease the lowering of the platform, but so far it has not been a vital objective.

All in all, the main issue seems to be the resin vat and the coating. The ripping effect is a problem even with a thick coating as one can observe from Fig. 9.4. However, based on previous experiments, there should not be any significant ripping if the exposure time is optimized (at least when a long penetration depth resin is used) [34]. The quality of the manufacturing experiments done in this study also suffered from the uneven bottom of the petri dish, since it notably complicated the exposure time optimization. As long as ripping is present, the fabrication process will always be complicated. In the previous experiments the ripping was neglected by moving the curing spot every couple of layers so that a defect did not have time to grow. However, this kind of an approach is not suitable since moving the curing spot causes irregularities in the curing layer thickness, as seen in Fig. 9.5. These defects are not so visible in Fig. 8.5(a), since the shape of each layer differs significantly from the previous one.

For future research a new resin vat should be made. The bottom must be even so that the exposure time can be optimized more reliably. So far PDMS has been the best coating material, since the attachment force to it is the smallest among those materials tested [34]. PDMS was also used by Pan *et al.* [26], who constructed a MIP-SLA for high-speed fabrication. They also developed a two-way movement design to reduce the separation force further and to keep high manufacturing speed. In addition to the vertical linear translator, they added a linear translator, to move the resin vat in the lateral direction. Adding the sideways movement to the process reduced the separation force to 3-4 % of the separation force with only vertical movement. This method directs the pulling force away from the normal of the

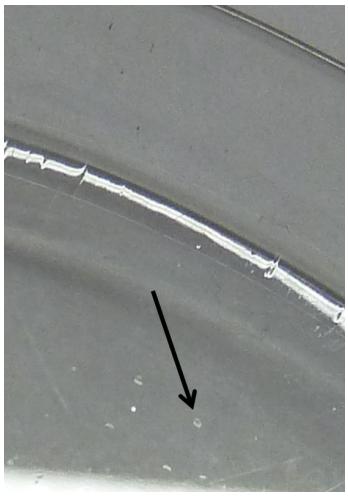

Figure 9.4: Pits caused by the cured resin ripping off from the thick PDMS coating, same petri dish as in Fig. 9.3.

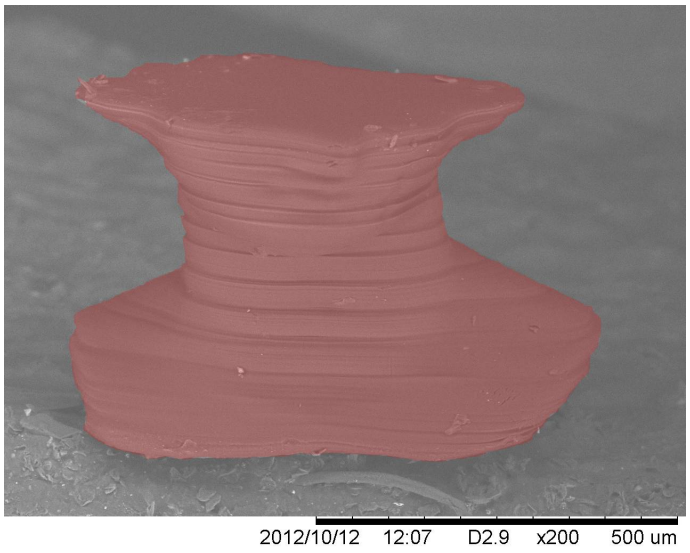

Figure 9.5: Irregularities in the layer fabrication due to changes in the curing spot position.

resin vat bottom. This can also be achieved by tilting the resin vat slightly before pulling up the platform, which is a known method used by some EnvisionTEC rapid prototyping systems. Thus, adding an extra linear translator to the PμSLA may also reduce the separation force. However, as the resin vat is moved sideways the curing spot changes, which may be a problem if any pits are formed on the coating or the coating thickness is not exactly the same for all spots. One should also remember that the MIP-SLA has worse fabrication accuracy than PμSLA, especially in the vertical direction. Changing the resin into a short penetration depth one, was the factor that lead to many fabrication difficulties in PμSL.

Despite the issues concerning the fabrication process with a short penetration depth resin, the construction of the PμSL equipment was successful. The computer program made to operate the process worked well, only the resin vat and the resin caused some challenges. These challenges can surely be overcome so that a true PμSL system, which produces objects with a few μm accuracy both in the vertical and lateral direction, can be constructed. Further research should focus on inhibiting the PDMS ripping so that repetition tests and small parameter adjustments can reliably be investigated.

In the future, μSL may become a suitable technology for medical and lab-on-a-chip applications. The research will continue in constructing a system capable of producing high-detail objects in an inexpensive way, and to look for new innovations.

References

[1] Emons, M., Obata, K., Binhammer, T., Ovsianikov, B., Chichkov, B. and Morgner, U. Two-photon polymerization technique with sub-50 nm resolution by sub-10 fs laser pulses. *Optical Materials Express,* 2012, vol. 2, issue 7, p. 942–947.

[2] Hutchinson, H. The Art of the Quick and Complex. Mechanical Engineering. Web document. April 2008. Referred to 6.2.2013. Available: `http://www.quickparts.com/UserFiles/File/http_www.memagazine.org_contents_current_webonly_wex04.pdf`.

[3] Junk, S., Sämann-Sun, J. and Niederhofer, M. Application of 3D printing for the Rapid Tooling of Thermoforming Moulds. in Hinduja, S. and Li, L. (ed.) *Proceedings of the 36th International MATADOR Conference,* Springer, 2010, p. 369–372.

[4] Gibson, I., Rosen, D. and Stucker, B. *Additive Manufacturing Technologies: Rapid Prototyping to Direct Digital Manufacturing.* Society of Springer, 2010.

[5] Bertsch, A., Zissi, S., Jézéquel, J., Corbel, S. and Andre, J. Microstereophotolithography using a liquid crystal display as dynamic mask-generator. *Microsystem Technologies,* 1997, vol. 3, issue 2, p. 42–47.

[6] Zhang, X., Jiang, X. and Sun, C. Micro-stereolithography of polymeric and ceramic microstructures. *Sensors and Actuators A,* 1999, vol. 77, no. 2, p. 149–156.

[7] Ikuta, K. and Hirowatari, K. Real Three Dimensional Micro Fabrication Using Stereo Lithography and Metal Molding. *Proceedings of IEEE International Workshop on Micro Electro Mechanical Systems,* 1993, p. 42–47.

[8] Moskvitch, K. Artificial blood vessels created on a 3D printer. BBC News. Web document. Updated 16.9.2011. Referred to 13.1.2013. Available: `http://www.bbc.co.uk/news/technology-14946808`.

[9] Chua, C., Leong, K. and Lim, C. *Rapid Prototyping: Principles and Applications.* Third edition, World Scientific, 2010.

[10] Jacobs, P. and Reid, D. *Rapid prototyping & manufacturing: fundamentals of stereolithography.* Society of Manufacturing Engineers, 1992.

[11] Anderson, C. *Makers: The New Industrial Revolution.* Random House Business Books, 2012.

[12] Rouse, S. *Advanced Trauma Surgery Using Additive Manufacturing.* Finnish Rapid Prototyping Association (FIRPA), Pikavalmistus - Materiaalia lisäävä valmistus (seminar), Otaniemi, 6.4.2011.

[13] Khoshnevis, B. *Automated construction by Contour Crafting.* Finnish Rapid Prototyping Association (FIRPA), Pikavalmistus - Materiaalia lisäävä valmistus (seminar), Otaniemi, 6.4.2011.

[14] Moskvitch, K. Printer produces personalised 3D chocolate. BBC News. Web document. Updated 5.7.2011. Referred to 16.1.2013. Available: `http://www.bbc.co.uk/news/technology-14030720`.

[15] Day, P. Will 3D printing revolutionise manufacturing?. BBC News. Web document. Updated 27.7.2011. Referred to 19.1.2013. Available: `http://www.bbc.co.uk/news/business-14282091`.

[16] Koskela, J. Light-induced biomaterial microfabrication for advanced cell culturing – a comparative study. Master of Science Thesis, Tampere University of Technology, Biomaterials, Tampere, 2010.

[17] Nguyen, K. and West, J. Photopolymerizable hydrogels for tissue engineering applications. *Biomaterials,* 2002, vol. 23, no. 22, p. 4307–4314.

[18] Fouassier, J. *Photoinitiation, photopolymerization, and photocuring: fundamentals and applications.* Hanser, 1995.

[19] Choi, J. Development of Projection-based Microstereolithography Apparatus, Adapted to Large Surface and Microstructure Fabrication for Human body Application. Doctoral dissertation, 2006.

[20] Rueggeberg, F. State-of-the-art: Dental photocuring – A review. *Dental Materials,* 2011, vol. 27, issue. 1, p. 39–52.

[21] Bertsch, A. and Renaud, P. Microstereolithography. in Bartolo, P. (ed.) *Stereolithography: Materials, Processes and Applications,* Springer, 2011, p. 81–112.

[22] Corbel, S., Dufaud, O. and Roques-Carmes, T. Materials for Stereolithography. in Bartolo, P. (ed.) *Stereolithography: Materials, Processes and Applications,* Springer, 2011, p. 141–157.

[23] Bartolo, P. Stereolithographic Processes. in Bartolo, P. (ed.) *Stereolithography: Materials, Processes and Applications,* Springer, 2011, p. 1–29.

[24] Madou, M. *Fundamentals of Microfabrication and Nanotechnology: Manufacturing techniques for microfabrication and nanotechnology, Volume II.* Third

edition, CRC Press, 2011.

[25] Sun, C., Fang, N., Wu, D. and Zhang, X. Projection micro-stereolithography using digital micro-mirror dynamic mask. *Sensors and Actuators A: Physical,* 2005, vol. 121, issue 1, p. 113–120.

[26] Pan, Y., Zhou, C. and Chen, Y. Rapid prototyping in minutes: the development of a mask projection stereolithography process for high-speed fabrication. *Proceedings of the ASME 2012 International Manufacturing Science and Engineering Conferences,* 2012.

[27] Ha, Y., Choi, J. and Lee, S. Mass production of 3-D microstructures using projection microstereolithography. *Journal of Mechanical Science and Technology,* 2008, vol. 22, issue 3, p. 514–521.

[28] Ikuta, K., Maruo, S., Hasegawa, T., Adachi, T., Takahashi, A., and Ikeda, K. Biochemical IC Chips Fabricated by Hybrid Microstereolithography. *MRS Proceedings,* 2002, vol. 758.

[29] Bertsch, A., Jiguet, S. and Renaud, P. Microfabrication of ceramic components by microstereolithography. *Journal of Micromechanics and Microengineering,* 2004, vol. 14, no. 2, p. 197–203.

[30] Maruo, S., Nakamura, O. and Kawata, S. Three-dimensional microfabrication with two-photon-absorbed photopolymerization. *Optics Letters,* 1997, vol. 22, no. 2, p. 132–134.

[31] Kawata, S., Sun, H., Tanaka, T. and Takada, K. Finer features for functional microdevices. *Nature,* 2001, vol. 412, , p. 697–698.

[32] Bertsch, A., Jézéquel, J. and Andre, J. Study of the spatial resolution of a new 3D microfabrication process: the microstereophotolithography using a dynamic mask-generator technique. *Journal of Photochemistry and Photobiology A: Chemistry,* 1997, vol. 107, p. 275–281.

[33] Farsari, M., Claret-Tournier, S., Huang, S., Chatwin, C., Budgett, P., Birch, P., Young, R. and Richardson, J. A novel high-accuracy microstereolithography method employing an adaptive electro-optic mask. *Journal of Materials Processing Technology,* 2000, vol. 107, p. 167–172.

[34] Lehtinen, P. Reducing the attachment force of cured resin to the resin vat in bottom-up stereolithography, Special Assignment, Aalto University School of Science, 2012.

[35] Stepper Online. Planetary Gearbox 14:1 for Nema 16 Geared Step-

per Motor. Web document. Referred to 15.1.2013. Available: http://www.stepperonline.com/16hs130604spg14-planetary-gearbox-141-for-nema-16-stepper-p-38.html.

[36] Lehtinen, P. Achieving micrometer resolution in stereolithography by utilizing neutral absorbers, Special Assignment, Aalto University School of Science, 2012.

[37] Budimir, M. Microstepping myths. Web document. Updated 9.10.2003. Referred to 13.1.2013. Available: http://machinedesign.com/article/microstepping-myths-1009.

[38] Karvinen, T. and Karvinen, K. *Sulautetut: Opi rakentamaan robotteja ja muita sulautettuja järjestelmiä.* Jyväskylä, Gummerus kirjapaino Oy, 2009.

A Source codes of the written programs

A.1 Code uploaded to Arduino Uno

The program uploaded to the Arduino Uno microcontroller is presented below with explanations.

```
#define DIR_PIN 2
#define STEP_PIN 3
//Numerical values

float t=22; //This value should match the microsteps required to move 1 micrometer
float L=10984; //movement distance upward after curing one layer, amount of microsteps,
//it should correspond to movement of about 0,5 mm
float v=0.5; //the ratio between upward and downward speed, up_s/do_s
float k=2; //distance moved after the part has been completed is k*L
float s1=0.2; // speed 0.2
float s2=0.5; // speed 0.5
float s3=1; // speed 1.0
float t1=1; // layer thickness 1 micrometer
float t2=2; // layer thickness 2 micrometers
float t3=5; // layer thickness 5 micrometers
float t4=10; // layer thickness 10 micrometers
float u; //product of t*ti
float p=110; //Used for motor jogging, 5 micrometers step
float w=4394; //Used for motor jogging, 200 micrometers step

//Changing the rotation direction: change the sign of L and t, they must have the same sign

char msg = '  ';   // a variable to hold data from serial

void setup() {
  pinMode(DIR_PIN, OUTPUT);
  pinMode(STEP_PIN, OUTPUT);
  Serial.begin(9600); //Activating DIR and STEP pins and setting data rate to 9600, for Arduino Uno
}

void loop(){
  // While data is sent over the serial port it is assigned to the msg
  while (Serial.available()>0){
    msg=Serial.read();
  }

  if (msg=='a') {
    u=t1*t;
    rotate(L, v*s1);
    rotate(-L+u, s1);
    msg=' '; //msg is cleared
```

```
42    }
43    else if (msg=='b') {
44      u=t1*t;
45      rotate(L, v*s2);
46      rotate(-L+u, s2);
47      msg=' ';
48    }
49    else if (msg=='c') {
50      u=t1*t;
51      rotate(L, v*s3);
52      rotate(-L+u, s3);
53      msg=' ';
54    }
55    else if (msg=='d') {
56      u=t2*t;
57      rotate(L, v*s1);
58      rotate(-L+u, s1);
59      msg=' ';
60    }
61    else if (msg=='e') {
62      u=t2*t;
63      rotate(L, v*s2);
64      rotate(-L+u, s2);
65      msg=' ';
66    }
67    else if (msg=='f') {
68      u=t2*t;
69      rotate(L, v*s3);
70      rotate(-L+u, s3);
71      msg=' ';
72    }
73    else if (msg=='g') {
74      u=t3*t;
75      rotate(L, v*s1);
76      rotate(-L+u, s1);
77      msg=' ';
78    }
79    else if (msg=='h') {
80      u=t3*t;
81      rotate(L, v*s2);
82      rotate(-L+u, s2);
83      msg=' ';
84    }
85    else if (msg=='i') {
86      u=t3*t;
87      rotate(L, v*s3);
88      rotate(-L+u, s3);
89      msg=' ';
90    }
91    else if (msg=='j') {
92      u=t4*t;
93      rotate(L, v*s1);
94      rotate(-L+u, s1);
95      msg=' ';
```

```
96    }
97    else if (msg=='k') {
98      u=t4*t;
99      rotate(L, v*s2);
100     rotate(-L+u, s2);
101     msg=' ';
102   }
103   else if (msg=='l') {
104     u=t4*t;
105     rotate(L, v*s3);
106     rotate(-L+u, s3);
107     msg=' ';
108   }
109   else if (msg=='x') {
110     rotate(k*L, v*s1);
111     msg=' ';
112   }
113   else if (msg=='y') {
114     rotate(k*L, v*s2);
115     msg=' ';
116   }
117   else if (msg=='z') {
118     rotate(k*L, v*s3);
119     msg=' ';
120   }
121   else if (msg=='m') {
122     rotate(p, v*s3);
123     msg=' ';
124   }
125   else if (msg=='o') {
126     rotate(-p, v*s3);
127     msg=' ';
128   }
129   else if (msg=='r') {
130     rotate(w, v*s3);
131     msg=' ';
132   }
133   else if (msg=='q') {
134     rotate(-w, v*s3);
135     msg=' ';
136   }
137   else if (msg=='n') {
138     digitalWrite(STEP_PIN, LOW); // turns motor off
139   }
140 }
141
142 void rotate(int steps, float speed){
143   //rotate a specific number of microsteps (in this case 8 microsteps
          per step)
144   //rotation speed is between 0.01 and 1, and 1 is max speed
145   int dir = (steps > 0)? HIGH:LOW;
146   steps = abs(steps);
147
148   digitalWrite(DIR_PIN, dir);
```

```
149
150   float sDelay = (1/speed) * 70; //Delay for adjusting rotation speed
151
152   for(int i=0; i < steps; i++){
153     digitalWrite(STEP_PIN, HIGH);
154     delayMicroseconds(sDelay);
155
156     digitalWrite(STEP_PIN, LOW);
157     delayMicroseconds(sDelay);
158   }
159 }
```

Two pins "DIR_PIN" and "STEP_PIN" are defined and activated. The Easy-Driver is connected to the Arduino via these two pins. Multiple numerical values are stored for controlling the movement distance and speed. The pins are set to output mode and the data rate is set to 9600 corresponding to the data rate used by Arduino Uno. When data is sent over the serial port it will be stored into the variable *msg*. The rotation method is defined at the end part of the code. The motor will be controlled by microsteps (8 microsteps per step). Thus, 21968 (2746×8) microsteps are required to make one full revolution. The rotation speed is set to vary between 0.01 and 1, where 1 corresponds to maximum speed. Since 21968 microsteps are required for one revolution, linear movement of 1 µm corresponds to about 22 (21968/1000) microsteps when a M6 threaded rod is used. The main loop in the program reads the *msg* and rotates the motor accordingly. The data received from the serial port is defined by the options made in the computer program presented in the next section. In this case, the data received will just be a letter. Once the letter has been read, the layer thickness and motor speed are stored accordingly. Each letter has its own combination of layer thickness and motor speed values. Then the program will rotate the motor and thus move the platform upward by 0.5 mm (10983 microsteps) and a slightly shorter distance downward, so that a small gap is created between the cured structure and the bottom surface of the resin vat. The program clears the message, stays put and waits for the next data value from the serial port.

A.2 Source code of the operation program

The source code of the program used for controlling the slideshow and giving commands to the Arduino Uno microcontroller is presented below with detailed explanations.

```
1  import wx, gtk, os, serial, gobject, time, sys, winsound
2  from time import clock
3  from wx.lib.masked import NumCtrl
4
5  # Global variables
6
7  dir="data"
8  pixbufs=[]
9  image=None
10 bg=None
11 pos=0
12 ser=None
13 counter=0 #layer counter
14 speed=0 #motor speed
15 layer=0 #determines the layer thickness
16 scaling=0 #stores the input value from image size radiobox
17 scaled=0 #determines the image scaling factor
18
19 ser = serial.Serial('COM4', 9600) #The serial port number must be set
       to 4 (Device Manager).
20
21 # Scale and center the image
22
23 def fitRect(thing, box):
24   # scale
25   global scaling
26
27   if scaling == 0:
28     scaled=1
29   elif scaling == 1:
30     scaled=0.75
31   elif scaling == 2:
32     scaled=0.5
33   elif scaling == 3:
34     scaled=0.25
35   elif scaling == 4:
36     scaled=0.125
37
38   scaleY=float(box.height)/thing.height
39   scaleX=float(box.width)/thing.width
40   scale=min(scaleY, scaleX)
41   thing.width=scaled*scale*thing.width
42   thing.height=scaled*scale*thing.height
43   # center
44   thing.x=box.width/2-thing.width/2
45   thing.y=box.height/2-thing.height/2
46   return thing
```

```
47
48 def scaleToBg(pix, bg):
49   fit=fitRect(
50     gtk.gdk.Rectangle(0,0, pix.get_width(), pix.get_height()),
51     gtk.gdk.Rectangle(0,0, bg.get_width(), bg.get_height())
52   )
53   scaled=pix.scale_simple(fit.width, fit.height, gtk.gdk.
       INTERP_BILINEAR)
54   ret=bg.copy()
55   scaled.copy_area(
56     src_x=0, src_y=0,
57     width=fit.width, height=fit.height,
58     dest_pixbuf=ret,
59     dest_x=fit.x, dest_y=fit.y
60   )
61   return ret
62
63 def newPix(width, height, color=0x000000ff):
64   pix=gtk.gdk.Pixbuf(gtk.gdk.COLORSPACE_RGB, True, 8, width, height)
65   pix.fill(color)
66   return pix
67
68 # Load images
69
70 def loadImages():
71   global pixbufs
72   for file in os.listdir(dir):
73     filePath=os.path.join(dir, file)
74     pix=gtk.gdk.pixbuf_new_from_file(filePath)
75     pix=scaleToBg(pix, bg)
76     pixbufs.append(pix)
77
78 # Change image
79
80 def go(relativePos):
81   global pos
82   last=len(pixbufs)-1
83   pos+=relativePos
84   if pos>last:
85     #When the part is complete: keep black image and play end.wav
86     image.set_from_pixbuf(pixbufs[0])
87     winsound.PlaySound("end.wav", winsound.SND_FILENAME)
88   image.set_from_pixbuf(pixbufs[pos])
89
90 def timer(*args):
91   global counter
92   counter=counter+1
93   image.set_from_pixbuf(pixbufs[0])
94   gtk.timeout_add((delay+movement)*1000, timer2)
95   if counter < len(pixbufs):
96     gtk.timeout_add(delay*1000, timer3)
97     return True
98   else:
99     return False
```

```
100
101 def timer2(*args):
102   go(1)
103   return False
104
105 def timer3(*args):
106   if speed == 0 and layer == 0:
107     ser.write('a')
108   elif speed == 1 and layer == 0:
109     ser.write('b')
110   elif speed == 2 and layer == 0:
111     ser.write('c')
112   elif speed == 0 and layer == 1:
113     ser.write('d')
114   elif speed == 1 and layer == 1:
115     ser.write('e')
116   elif speed == 2 and layer == 1:
117     ser.write('f')
118   elif speed == 0 and layer == 2:
119     ser.write('g')
120   elif speed == 1 and layer == 2:
121     ser.write('h')
122   elif speed == 2 and layer == 2:
123     ser.write('i')
124   elif speed == 0 and layer == 3:
125     ser.write('j')
126   elif speed == 1 and layer == 3:
127     ser.write('k')
128   elif speed == 2 and layer == 3:
129     ser.write('l')
130   else:
131     ser.write('n')
132   ser.write('n')
133   return False
134
135 def keyEvent(widget, event):
136   global pos, counter, image
137   key = gtk.gdk.keyval_name(event.keyval)
138   if key=="space" or key=="Page_Down":
139     go(1)
140   elif key=="Page_Up":
141     if speed == 0:
142       ser.write('x')
143     elif speed == 1:
144       ser.write('y')
145     elif speed == 2:
146       ser.write('z')
147     ser.write('n')
148   elif key=="s":
149     gtk.timeout_add((delay+movement+exposure)*1000, timer)
150   elif key=="Escape":
151     sys.exit(0)
152
153 class ExamplePanel(wx.Frame):
```

```
154   def __init__(self, parent, mytitle, mysize):
155     wx.Frame.__init__(self, parent, -1, mytitle, size=mysize)
156
157     self.panel=wx.Panel(self,-1)
158     self.SetBackgroundColour("white")
159     self.quote = wx.StaticText(self, label="Insert wanted parameters
          and start the program.", pos=(20, 30))
160     self.quote = wx.StaticText(self, label="Once the curing is complete
           press Page Up to lift up the stage.", pos=(50, 350))
161     self.quote = wx.StaticText(self, label="Quit the program by
          pressing the Esc key.", pos=(50, 380))
162     self.quote = wx.StaticText(self, label="These buttons can be used
          to control the motor", pos=(120, 435))
163     self.quote = wx.StaticText(self, label="with 5 and 200 micrometers/
          step.", pos=(120, 455))
164 # Buttons
165     self.button =wx.Button(self, label="Press this button and then the
          s key", pos=(100, 310))
166     self.Bind(wx.EVT_BUTTON, self.OnClick, self.button)
167
168     self.button2 =wx.Button(self, label="Move up (5)", pos=(100, 480))
169     self.Bind(wx.EVT_BUTTON, self.OnClick2, self.button2)
170
171     self.button3 =wx.Button(self, label="Move down (5)", pos=(95, 520))
172     self.Bind(wx.EVT_BUTTON, self.OnClick3, self.button3)
173
174     self.button4 =wx.Button(self, label="Move up (200)", pos=(250, 480)
          )
175     self.Bind(wx.EVT_BUTTON, self.OnClick4, self.button4)
176
177     self.button5 =wx.Button(self, label="Move down (200)", pos=(245,
          520))
178     self.Bind(wx.EVT_BUTTON, self.OnClick5, self.button5)
179
180     self.lblname = wx.StaticText(self, label="Exposure time (s) :", pos
          =(20,60))
181     self.lblname2 = wx.StaticText(self, label="Delay (s) :", pos
          =(20,90))
182     self.lblname3 = wx.StaticText(self, label="Movement (s) :", pos
          =(20,120))
183     self.editname = wx.TextCtrl(self, -1, pos=(150, 60), size=(60,-1))
184     self.editname2 = wx.TextCtrl(self, -1, pos=(150, 90), size=(60,-1))
185     self.editname3 = wx.TextCtrl(self, -1, pos=(150, 120), size=(60,-1)
          )
186     self.Bind(wx.EVT_BUTTON, self.OnClick, self.button)
187
188 # Selecting speed
189     speed = ['0.2', '0.5', '1.0']
190     rb = wx.RadioBox(self, label="Motor speed", pos=(100, 200), choices
          =speed,  majorDimension=3,
191                              style=wx.RA_SPECIFY_COLS)
192     self.Bind(wx.EVT_RADIOBOX, self.EvtRadioBox, rb)
193
194 # Selecting layer thickness
```

```
195     thickness = ['1', '2', '5', '10']
196     rb2 = wx.RadioBox(self, label="Layer thickness (micrometers)", pos
            =(100, 250), choices=thickness,  majorDimension=4,
197                               style=wx.RA_SPECIFY_COLS)
198     self.Bind(wx.EVT_RADIOBOX, self.EvtRadioBox2, rb2)
199
200 # Scaling image
201     scaler = ['1:1', '3:4', '1:2', '1:4', '1:8']
202     rb3 = wx.RadioBox(self, label="Image size (1:1 is fullscreen)", pos
            =(100, 150), choices=scaler,  majorDimension=5,
203                               style=wx.RA_SPECIFY_COLS)
204     self.Bind(wx.EVT_RADIOBOX, self.EvtRadioBox3, rb3)
205
206   def EvtRadioBox(self, event):
207     global speed
208     speed = event.GetInt()
209
210   def EvtRadioBox2(self, event):
211     global layer
212     layer = event.GetInt()
213
214   def EvtRadioBox3(self, event):
215     global scaling
216     scaling = event.GetInt()
217
218   def OnClick(self,event):
219     global bg, image, ser, exposure, delay, movement
220     values=[]
221
222     values.append(int(self.editname.GetValue()))
223     values.append(int(self.editname2.GetValue()))
224     values.append(int(self.editname3.GetValue()))
225     exposure=values[0]
226     delay=values[1]
227     movement=values[2]
228     main()
229     app1()
230
231   def OnClick2(self,event):
232     ser.write('m')
233
234   def OnClick3(self,event):
235     ser.write('o')
236
237   def OnClick4(self,event):
238     ser.write('r')
239
240   def OnClick5(self,event):
241     ser.write('q')
242
243 class app1:
244
245   def __init__(self):
246     window = gtk.Window()
```

```
247       window.connect("destroy", gtk.main_quit)
248       window.connect("key-press-event", keyEvent)
249       window.connect("realize", self.realize_cb)
250       window.show_all()
251       window.fullscreen()
252       window.add(image)
253       window.show_all()
254
255 # Hiding the mouse cursor
256     def realize_cb(self, widget):
257       pixmap = gtk.gdk.Pixmap(None, 1, 1, 1)
258       color = gtk.gdk.Color()
259       cursor = gtk.gdk.Cursor(pixmap, pixmap, color, color, 0, 0)
260       widget.window.set_cursor(cursor)
261
262 def main():
263     global bg, image, ser
264     bg=newPix(gtk.gdk.screen_width(), gtk.gdk.screen_height())
265     loadImages()
266     image=gtk.image_new_from_pixbuf(pixbufs[pos])
267
268     app1()
269     gtk.main()
270
271 app = wx.App(False)
272 mytitle = 'Stereolithography'
273 width = 450
274 height = 600
275 ExamplePanel(None, mytitle, (width, height)).Show()
276 app.MainLoop()
277
278 if __name__ == "__main__":
279     main()
```

First multiple global variables are stored. The serial port communication is set to use port COM4 at 9600 data rate. The images are loaded from the folder *data* and they are scaled, centered and the background is filled with black. The scaling values are achieved from the radio buttons in the GUI. The image changing method *go* is defined. The position value of the images increases after each loop, i.e., after every cured layer. Once all the images have been displayed, the first file in the data folder will be displayed and a sound file "end.wav" will be played to notify the user that the manufacturing process is complete.

Timer methods are used repeatedly to control the timings between the platform movement and the image changing. The first *timer* keeps the screen black while the motor is moving, i.e., for the duration *delay*+*movement*, where *delay* and *movement* are values filled in the cells of the GUI. After this pause, *timer2* will be executed, which changes the projected image. If the counter in *timer* has not gone through all the images, *timer3* will be executed. Depending on the selected speed and layer thickness, a different letter is sent to the serial port. Each letter is a combination of

speed and layer thickness. The *timer* is a loop that is executed as long as it returns the value *True*. Once all the images have been executed, it will return *False* and the loop will stop.

The *keyEvent* method operates when specific keyboard keys are pressed. Pressing space or Page Down will change the projected image by one step. Page Up will move the platform upward. The part manufacturing process is started by pressing the s key and the program is shut down by pressing Esc. Once the s key is pressed the program will wait for *delay*+*movement*+*exposure* seconds and execute *timer*. Thus, *timer* is run every *delay*+*movement*+*exposure* seconds until all the images have been displayed.

The combination of the three timers, mentioned above, means that the image will be displayed for the duration *exposure*, the motor will be moved during the interval given by *movement* and *delay* is for extra waiting time before and after the image has been displayed. A small delay is used to make sure that the resin has settled down and no liquid movement is present when the curing process initiates.

The class *ExamplePanel* contains all the information regarding the GUI. The result is shown in Fig. 7.18. Exposure time, delay, movement, image scaling factor, motor speed and layer thickness values are all stored in variables when the large button in the middle of the GUI is pressed, i.e., *OnClick* is executed. *OnClick* will also activate the class *app1* and start the main loop. These involve loading of all the essential things required for running the slideshow and the motor movement part of the program. The mouse cursors is also made transparent in *app1*, since otherwise the shape of the cursor will be cured.

A Windows executable file can be created from the Python script. Thus, the user does not need to have Python installed, since the program is started by running an .exe file. The images received from the STL model slicing are placed in a folder named *data*. In the folder is also a black image named "00000.jpg", which is displayed during motor movement. The naming of images in the data folder should be such that the black image is first and the rest are in alphabetical order starting with the very bottom layer and ending with the top layer.

The user has to define the USB port that the Arduino Uno microcontroller is connected to as COM4 for the program to function. This can be done by using the Device manager in Windows environment. The naming of serial ports is different in Linux environment, which would lead to alterations in the source code [38].